EXTREME FRACTIONATION IN A GRANITE-PEGMATITE SYSTEM DOCUMENTED BY QUARTZ CHEMISTRY: THE CASE STUDY OF TRES ARROYOS (CENTRAL IBERIAN ZONE, SPAIN)

Garate-Olave, I.[1], Müller, A.[2,3], Roda-Robles, E.[1], Gil-Crespo, P.P.[1], Pesquera, A.[1]

1. Dpto. Mineralogía y Petrología, Univ. País Vasco-UPV/EHU, Apdo. 644, 48080-Bilbao, Spain,

2. Natural History Museum, University of Oslo, PO Box 1172, Blindern, Oslo 0318, Norway

3. Natural History Museum, Cromwell Road, London SW7 5BD, UK

*Corresponding author. E-mail address: idoia.garate@ehu.eus (I. Garate-Olave)

ABSTRACT

The Tres Arroyos granite-pegmatite system is located in the SW margin of the Nisa-Alburquerque Variscan batholith. Two granitic facies (monzogranite and marginal leucogranite), and three types of aplite-pegmatite dykes (barren, intermediate and highly evolved Li-rich), have been distinguished in the area, with a zoned distribution from the granite southwards. Trace elements in quartz from the five facies have been analyzed by LA-ICP-MS in order to obtain information about the petrogenetic links among the different lithologies of this system, as well as to better understand the regional and individual fractionation processes that led to the distinct rocks. Aluminium, Ti, Li and Ge show continuous trends from the monzogranite, through the marginal granitic facies, the barren and intermediate aplite-pegmatites, up to the most evolved Li-rich dykes.

Titanium and Ge contents, respectively, decrease and increase gradually with fractionation. In contrast, Al and Li show a more complex trend, with an initial descending trend to the marginal granitic facies, and then showing the highest Al and Li contents in the quartz from the most fractionated Li-rich aplite-pegmatites. This suggests the influence of different competing factors controlling the incorporation of these trace elements in quartz, such as the chemical composition of the melt, the P and T conditions and the rate of crystallization. Based on the good correlation between Al and Li, the substitution $Si^{4+} \Leftrightarrow Al^{3+} + Li^{+}$ seems to be the dominant mechanism of Li incorporation into quartz. The negligible amount of other trace elements suggests that the remaining Al was mainly compensated with H^{+} ions, via the $Si^{4+} \Leftrightarrow Al^{3+} + H^{+}$ substitution.

A continuous fractionation trend from the monzogranite up to the most fractionated aplite-pegmatites is inferred from geochemical modelling by applying the Rayleigh equation for fractional crystallization. Fractionation rates over 50% are needed to obtain the marginal granite and the barren aplite-pegmatites compositions, and over 99% for the most evolved dykes. No pattern in the chemical variation of the trace elements in quartz from different layers in the layered aplite-pegmatites has been found, suggesting the lack of internal fractionation processes, most probably due to the rapid crystallization of the pegmatitic melt, intruded into a colder country rock.

Keywords: quartz, trace elements, LA-ICP-MS, aplite-pegmatites, granites, Tres Arroyos, Central Iberian Zone

1. Introduction

51 Quartz is a rock-forming mineral in silica-saturated igneous rocks including granitic
52 pegmatites. Because of its abundance and the technical development of micro-analytical
53 methods, the trace element content of quartz has been utilized in the last two decades
54 for gaining information about the parental signature and the fractionation degree of the
55 melt from which the quartz crystallized. However, trace element studies of igneous
56 quartz are not very abundant (Schrön et al., 1988; Larsen et al., 2004; Müller et al.,
57 2008, 2015; Jacamon and Larsen, 2009; Breiter and Müller, 2009; Beurlen et al., 2011;
58 Breiter et al., 2013; Drivenes et al., 2016) in comparison to other minerals such as
59 feldspar, micas or tourmaline (Černý and Burt 1984; Foord et al., 1995; Larsen, 2002;
60 Roda et al., 2007; Vieira et al. 2011, Marchal et al., 2014*),* due to the very low
61 concentrations of trace elements in quartz and the related analytical challenges.
62 Quartz has a strong atomic bond between Si-O allowing only some elements to enter
63 the lattice in small concentrations (Rusk, 2012). Lithium, H, Be, B, Mn, Ge, Rb, Sr, Na,
64 Al, P, K, Ca, Ti, and Fe are the most common trace elements in natural quartz (e.g.,
65 Larsen et al., 2004; Götze et al., 2004; Rusk et al., 2008; Müller and Koch-Müller,
66 2009; Müller et al., 2010; Rusk, 2012). Each element either enter crystal lattice, or is in
67 the interstices. Common substitutional impurities are, Al^{3+}, Ti^{4+} or Ge^{4+}, and interstitial
68 impurities are K^{+}, Na^{+} or Li^{+} (Rusk, 2012). ICP-MS analyses of dissolute quartz were
69 already done on quartz since the late 1980's, early 1990's (Schrön et al., 1988).
70 However, techniques to analyse very low concentrations of trace elements in quartz *in*
71 *situ* (within individual crystals) were not available until the beginning of the 21st
72 century. The last two decades laser ablation combined with inductively coupled plasma
73 mass spectrometry (LA-ICP-MS) is applied for performing analysis of quartz $\mu g g^{-1}$ to
74 $n g g^{-1}$ range.

In this study quartz from the late-Variscan granite-pegmatite system from the Tres Arroyos area (Alburquerque, Badajoz), in SW Spain, is investigated. There, besides different granitic facies belonging to the Alburquerque batholith, a number of aplite-pegmatite bodies occur, with different degrees of evolution, some of them enriched in Li-F. Quartz from granites and aplite-pegmatites has been analysed by LA-ICP-MS, combined with the scanning electron microscope cathodoluminescence (SEM-CL), in order to establish the petrogenetic links among the different lithologies constituting the Tres Arroyos granite-pegmatite system. Geochemical modelling applying Rayleigh equations for fractional crystallization has been used for interpretation of the results obtained by LA-ICP-MS of quartz. In addition, the results of the trace element study were applied to reconstruct the internal chemical evolution of some pegmatite bodies. There are previous studies on the variations in the trace elements contents in igneous quartz from granitic rocks with different fractionation degrees (e.g., Breiter and Müller, 2009; Jacamon an Larsen, 2009; Breiter et al., 2012; 2013; Müller et al., 2003; 2005; Drivenes et al., 2016); and also on the trace elements in quartz from pegmatitic rocks of different types (e.g., Larsen et al., 2004; Müller et al., 2008; Beurlen et al., 2011; Müller et al, 2015). Despite Jacamon and Larsen (2009) already described the gradual change of chemistry in a layered granitic pluton that fractionated from ortopyroxene and clinopyroxene-bearing granite, over hornblende and biotite-granite, to aplogranitic layers, pegmatites, aplites, and finally hydrothermal veins, this is the first time where a study of the chemical quartz variations for a complete fractionation trend from granitic to highly evolved Li-rich pegmatitic facies is presented.

2. Geological setting and rock description

100 The Late-Variscan Tres Arroyos granite-pegmatite system is located to the south of
101 the Central-Iberian-Zone of the Variscan Massif, near to the limit with the Ossa Morena
102 Zone. The Tres Arroyos area occurs to the SW of the easternmost part of the Nisa-
103 Alburquerque (NA) batholith (Fig. 1). This batholith intruded into a Precambrian low-
104 grade metasedimentary sequence, including phyllites, slates, schists, quartzites and
105 metagreywackes belonging to the metamorphic Schist-Greywacke Complex (SGC).
106 Cordierite is the only contact metamorphic mineral developed together with a high
107 temperature biotite as a result of the granite thermal input (González-Menéndez et al.,
108 2010). The main facies of the NA batholith corresponds to a peraluminous
109 monzogranite, with minor two-mica leucogranitic facies (González-Menéndez, 1998).
110 Quartz, K-feldspar, plagioclase, biotite and muscovite are the main minerals, with
111 andalusite and cordierite, apatite and tourmaline as minor phases (Table 1). The
112 monzogranite shows a porphyritic texture, although locally it may be equigranular. In
113 the Tres Arroyos area the batholith exhibits a marginal facies (Gallego-Garrido, 1992)
114 characterized by a finer grain size, a higher abundance of tourmaline and certain
115 enrichment in F, Li and Fe in the muscovite. The emplacement conditions for the
116 monzogranite was ≤ 2.5 kbars (González-Menéndez et al., 2010) and the emplacement
117 age of 307-309 Ma (U-Pb, Solá et al., 2009). Regarding the Variscan deformation, this
118 granite is considered to be late- to post-tectonic.
119 Besides these granitic rocks, in the Tres Arroyos area three different kinds of aplite-
120 pegmatite bodies are observed, all of them intruded into metasediments of the SGC:
121 barren, intermediate, and evolved aplite-pegmatites (Table 1, Fig. 1). The barren bodies
122 are layered aplite-pegmatites that outcrop near the NA batholith (Fig. 1), which show a
123 N135E direction, dipping towards NE (Gallego-Garrido, 1992). Locally it is not easy to
124 distinguish in the field the marginal granitic facies from these barren aplite-pegmatites

due to the bad quality of the outcrops and to the similarities in hand-sample, but 15 bodies belonging to this type may be recognized in the field. The main mineralogical differences between the two lithologies are the lack of biotite and the occurrence of Fe-Mn phosphates in the aplite-pegmatites. Moreover, the meteoric alteration of the phosphates gives frequently a characteristic greenish color to some of these dykes. Micas from barren aplite-pegmatites are usually richer in F, Li and Fe than the muscovite from the marginal granitic facies, belonging to the muscovite- zinnwaldite series. The grain size changes from 0.1 to 3 cm. Some of the dykes show just aplitic facies, whereas in other cases aplitic and pegmatitic layers are present.

The intermediate bodies correspond to sub-horizontal, discordant, leucocratic aplite-pegmatite dykes, with up to 8 meters of thickness. In the field 7 intermediate dykes have been localized. These bodies are mainly composed of albite and quartz, with K-feldspar and micas as minor minerals, and topaz, Li-Al-phosphates and Nb-Ta-Sn-oxides as accessory phases. Some of these bodies display a rhythmical layering, where albite-rich layers alternate with quartz-rich ones (Fig. 2a).

Evolved lithium-rich aplite-pegmatites constitute the third category. According to previous studies and the present work, there are around a dozen of Li-F-rich aplite-pegmatite bodies in the studied area. They show an important enrichment in Li and F, reflected in their mineral association that includes Li-rich micas, topaz and montebrasite. As the other aplite-pegmatite types, some of these Li-rich dykes show different layering patterns, with layers rich in Li-micas alternating with quartz + albite rich ones (Fig. 2b).

3. Sampling and analytical methods

Thirteen representative samples of quartz were selected for textural and geochemical characterization, from the five different facies distinguished in the Tres Arroyos area. The quartz samples were prepared as surface-polished, 300-µm thick sections mounted on standard glass slides.

Scanning electron microscope cathodoluminescence (SEM-CL) images of quartz were obtained from the thick sections coated with carbon using the LEO 1450VP analytical SEM with an attached CENTAURUS BS BIALKALI type cathodoluminescence (CL) detector. The applied acceleration voltage and current at the sample surface were 20 kV and ~3 nA, respectively. The BIALKALI tube has a CL response range from 300 (violet) to 650 nm (red). It peaks in the violet spectrum range around 400 nm. The CL images were collected from one scan of 43s photo speed and a processing resolution of 1024 × 768 pixels and 256 grey levels. SEM-CL was applied to quartz in order to reveal intra-crystal, micro-scale (<1 mm) growth zonation and alteration structures and different quartz generations. Grey-scale contrasts visualized by SEM-CL are caused by the heterogeneous distribution of lattice defects (e.g., oxygen and silicon vacancies, broken bonds) and trace elements in the quartz lattice (e.g., Sprunt, 1981; Ramseyer et al., 1988; Perny et al., 1992; Stevens Kalceff et al., 2000; Götze et al., 2001; 2004; 2005). Although the physical background of the quartz CL is not fully understood, the structures revealed by CL give information about crystallization, deformation and fluid- driven overprint.

Concentrations of Li, Be, B, Mn, Ge, Rb, Sr, Na, Al, P, K, Ca, Ti, and Fe in quartz were determined with the laser ablation-inductively coupled plasma-mass spectrometry (LA-ICP-MS) technique. One of the advantages of this method is that the quartz crystals are analyzed *in situ,* meaning distinct parts of a crystal can be chosen for analyses. Nevertheless, micro fluid and mineral inclusions have to be avoided to make

175 sure that the obtained trace element concentrations represent lattice-bound and
176 interstitial elements. 58 quartz analyses were undertaken on a double-focusing sector
177 field inductively coupled plasma mass spectrometer, HR-SF-ICP-MS, model
178 ELEMENT XR from Thermo Scientific, which is linked to an excimer laser probe New
179 Wave UP193FX ESI. The 193-nm laser had a repetition rate of 20 Hz, a spot size of 50
180 μm, and energy fluence about 5 to 6 $J \cdot cm^{-2}$ on the sample surface. A continuous raster
181 ablation on an area of approximately 150 × 400 μm was applied.
182 The approximate depth of ablation was between 10 and 50 μm. An Hitachi CCD
183 video camera, type KP-D20BU, attached to the laser system, was used to observe the
184 laser ablation process and to avoid the analyses of micro mineral and fluid inclusions.
185 Occasionally, however, individual fluid inclusions were hit, where it was not possible to
186 find crystal domains entirely free of fluid inclusions. These analyses are recognizable
187 from concentration spikes for Na, K, and/or Ca.
188 The carrier gas for transport of the ablated material to the ICP-MS was He mixed
189 with Ar. The isotope ^{29}Si was used as the internal standard applying the stoichiometric
190 concentration of Si in SiO_2. External multistandard calibration was performed using
191 NIST SRM 610, 612, and 614 and NIST SRM 1830 soda-lime float glass (0.1% m/m
192 Al_2O_3), the certified reference material BAM No. 1 amorphous SiO_2 glass from the
193 Federal Institute for Material Research and Testing in Germany, and the Qz-Tu
194 synthetic pure quartz monocrystal provided by Andreas Kronz from the
195 Geowissenschaftliches Zentrum Göttingen (GZG), Germany. Certified, recommended,
196 and proposed values for these reference materials were taken from Jochum et al. (2011)
197 and from the certificates of analysis where available. For the calculation of P
198 concentrations, the procedure of Müller et al. (2008) was applied.

Each measurement comprised 15 scans of each isotope, with the measurement time varying from 0.15 s/scan for K in medium mass resolution mode to 0.024 s/scan of, Li in low mass resolution mode. An Ar blank was run before each reference material and sample measurement to determine the background signal. The background was subtracted from the instrumental response of the reference material/ sample before normalization against the internal standard in order to avoid effects of instrumental drift. This was carried out to avoid memory effects between samples. A weighted least squares regression model, including several measurements of the six reference materials, was used to define the calibration curve for each element. Ten sequential measurements on the BAM No.1 SiO_2 quartz glass were used to estimate the limits of detection (LOD) which were based on 3 × standard deviation (3σ) of the 10 measurements. LODs are listed in Table 2.

14 representative bulk samples of aplite-pegmatites were analyzed for trace elements, including Ba as compatible and Li, Rb and Cs as incompatible elements. These data were obtained by X-ray fluorescence (XRF) and ICP-MS at the Activation Laboratories Ltd. (Actlabs, Canada).

4. Results

4.1. Micro-textures in cathodoluminescence images of quartz

Quartz occurs in plutonic rocks as fine-grained crystals, homogeneously distributed. Under the microscope it appears as anhedral, granular grains, most commonly exhibiting undulose extinction. In the aplite-pegmatite dykes, quartz occurs also as anhedral crystals with a much more variable grain size, from medium-sized grains (up

to 3 cm) in the pegmatitic layers to finer grains (200-1000 μm) in the aplitic ones. Quartz is the only phase in some layers, whereas in others it coexists with feldspars, micas and, less commonly, phosphates. Quartz also appears as small inclusions (<2 mm) in schorl.

In general, quartz crystals from the Tres Arroyos area appear very homogeneous in SEM-CL images (Fig. 3a). Only one sample from a simply layered unit of an intermediate pegmatite shows a weakly-contrasted growth zoning (Fig. 3b). The general lack of primary growth zoning and the very low CL contrasts may indicate that trace elements are homogeneously distributed within the quartz crystals. Also the abundance of secondary microstructures is relatively low in the Tres Arroyos quartz, comparing with quartz associated with pegmatites from other localities (e.g., Larsen et al., 2004; Müller et al., 2008; Drivenes et al., 2016). Only a few thin (<5 μm), intra and transgranular healed cracks, connecting non-luminescent domains, were observed in some quartz crystals from layered intermediate (Fig. 3c) and Li-rich (Fig. 3d) dykes.

4.2. Trace elements in quartz from aplite-pegmatites and granites

For LA-ICP-Ms analyses, relative coarse, clear crystals (>1 mm) were chosen due to the applied laser raster technique (150 × 400 μm). In the layered pegmatites the choice of quartz crystals was more difficult, in particular in the aplitic layers, due to the small grain size. There sometimes it was not always possible to avoid the contamination of the analyses by fluid inclusions. In those cases the Na, K, Ca, P and Fe values may be anomalously high and, thus, the determined concentrations may not correspond to the concentration of lattice-bound trace elements. For example, the presence of NaCl-bearing fluid inclusions in quartz is indicated by concentration pikes of Na (up to 240

μgg^{-1}) compared to the average lattice-bound content of 1-5 μgg^{-1}. In order to exclude all the point analyses that could be contaminated by fluid inclusions, only Na values <10 μgg^{-1} have been taken into account. On the other hand, micro apatite inclusions may be also identified in some analyses from intermediate aplite-pegmatites and lithium rich dykes owing to P high values (up to 30 μgg^{-1}). The rest of analyses commonly show P contents under 10 μgg^{-1}.

Data obtained by LA-ICP-MS are given in Table 3. In Fig. 4 representative trace element binary plots are provided, illustrating variations in the trace element contents of quartz from different granites and pegmatites. Besides Al and Ti, which are generally the most common trace elements in igneous quartz, Li contents are relatively high in most of the analyzed quartz crystals from Tres Arroyos.

Concentrations of Al are in the range 132-854 μgg^{-1} (Fig. 4a, b), with a continuous but not rectilinear variation from the less to the most fractionated lithologies (Table 3, Fig. 4a and b). The monzogranite shows intermediate values (258-540 μgg^{-1}), whereas the marginal granitic facies and the barren aplite-pegmatites show lower Al contents (165-263 μgg^{-1} and 160-297 μgg^{-1}, respectively). There is an increase in the intermediate bodies (132-653 μgg^{-1}); and finally, the highest values are found in the quartz from the Li-rich aplite-pegmatites (324-854 μgg^{-1}) (Table 3, Fig. 4a, b). In contrast, there is a continuous decrease in the Ti contents from the monzogranite to the Li-bearing dykes; through the intermedidate lithologies, with values in the ranges 50-134 μgg^{-1} for the monzogranitic facies, 5-30 μgg^{-1} for the marginal granite, 5-15 μgg^{-1} for the barren aplite-pegmatites, 1-5 μgg^{-1} for the intermediate aplite-pegmatites, and <2 μgg^{-1} for the Li-rich dykes (Fig. 4a, c). The contents of Li in the quartz from the five different facies vary between 14-134 μgg^{-1} (Fig. 4b). As expected, the highest values are found in the Li-rich dykes (45-134 μgg^{-1}). Nevertheless, the other values are also

quite high, in the range 35-71 μgg^{-1} for the monzogranite, 36-43 μgg^{-1} for the marginal granite, 31-47 μgg^{-1} for the barren dykes, and 14-80 μgg^{-1} for the intermediate aplite-pegmatites. Aluminium and Li show a significant positive correlation (Fig. 4b), which is due to the incorporation of both elements via the substitution $Si^{4+} \Leftrightarrow Al^{3+} + Li^{+}$, where Al replaces Si in the tetrahedral site, whereas the small Li ions occur in interstitial lattice position (Dennen, 1966). Germanium values are in the range of 0.99-6.35 μgg^{-1}. The lowest values are related to the monzogranite facies, not exceeding 2 μgg^{-1}. Taking into account the average values, there is a Ge enrichment from the monzogranite, through the marginal granite, barren and intermediate dykes, up to the lithium aplite-pegmatites, with values >1.5 μgg^{-1} for the marginal granite and the three types of aplite-pegmatites, which are values typical of pegmatite quartz (Götze et al., 2004) (Table 3, Fig. 4c). Boron values vary over a wide range in each type of bodies, with the lowest values associated with the monzogranite (1-2 μgg^{-1}), and the highest with the Li-rich dykes (2-7 μgg^{-1}) (Table 3, Fig. 4d). The Be contents are generally low (<1 μgg^{-1}), in the range 0.01-0.52 μgg^{-1}, achieving the highest values also in the Li-rich dykes. Iron values for the quartz from the monzogranite change from 5 to 49 μgg^{-1}, which are in the range of the S type granites. These are considerably high when compared to the contents in the I type granites (Breiter et al., 2013). In contrast, the marginal granitic facies and the different aplite-pegmatite dykes exhibit low Fe (<1 μgg^{-1}) (Table 3).

The Al/Ti and Ge/Ti ratios in quartz, good indicators of the degree of fractionation of the parental melt (e.g., Jacamon and Larsen, 2009; Breiter et al., 2012, 2013; Drivenes et al., 2016), show a clear positive correlation, with the lowest values belonging to the monzogranite and the highest to the Li-rich dykes (Fig. 4d).

In order to check if there is a correlation between the trace elements contents in quartz and the bulk composition of its hosting rock, the values of Al, Ti, Li and Ge in quartz (mean values for every sample), versus the contents of those elements in the bulk rock have been plotted (Fig. 5). Titanium is the only element with a clear positive correlation among the quartz and the bulk rock contents. Aluminium and Li show the highest contents in the most fractionated and most peraluminous Li-rich aplite-pegmatites, whereas the lowest values of Ge in both, quartz and whole rock, belong to the monzogranite samples. A correlation between the quartz contents and the bulk rock composition is not evidenced for these elements in the rest of the facies. The Al/Ti vs Ge/Ti values for the whole rock data have been also plotted in order to compare to the trend of these values in quartz, obtaining a similar result, with a relatively good positive correlation between the two sets of data, and a gradual increase from the monzogranite to the Li-rich aplite-pegmatites (Fig. 5e).

Some of the investigated aplite-pegmatite bodies show a layered structure, whereby coarse-grained comb-textured layers alternate with aplitic layers. Quartz from different layers has been analyzed to examine if there are differences in the trace element content of quartz in order to better understand the internal evolution of the dykes. Quartz analyses are summarized in Table 4. The Al and Li contents are in general lower in the aplitic layers than in the pegmatitic ones, whereas the Ti and P concentration in quartz seems to be independent from the facies. Some samples have slightly higher Ge contents in the coarse quartz crystals. During crystallization no variation in the contents of trace elements is noticed from the contacts inward the dykes.

4.3. Bulk rock trace element modelling

323 Different models have been proposed to explain the origin of highly evolved
324 pegmatitic melts, mainly including fractional crystallization of granitic magmas (e.g.,
325 London 2008; Vieira 2010), partial melting of metasediments (e.g., Norton, 1973;
326 Stewart, 1978; Sokolov, 1982; Shmakin, 1983; Simmons et al., 1995; Simmons and
327 Webber, 2008; Novak et al., 2013; Shaw et al., 2016; Simmons et al., in press) and a
328 combination of these two mechanisms (Jolliff et al., 1992; Roda-Robles, 1993).
329 Fractional crystallization is the most accepted mechanism to understand the "exotic"
330 composition of some pegmatites, starting from a granitic composition.
331 A geochemical modelling has been made in order to evaluate the petrogenetic
332 relationships between the Nisa-Alburquerque granite and the aplite-pegmatites from
333 Tres Arroyos. This modelling is developed starting from the whole-rock data on Ba, Rb
334 and Li of the Nisa-Alburquerque monzogranitic facies, by applying the Rayleigh
335 equation for fractional crystallization (Neumann, 1954):

336 $$C_1/C_0=F^{(D-1)}$$

337 where C_1 is the concentration (ppm) of trace elements in the melt at different degrees of
338 fractionation, C_0 is the concentration (ppm) of the elements in the parental melt (the
339 Nisa-Alburquerque granite); F is the fractionation degree and D represents the partition
340 coefficients between the melt and the forming minerals of the granite, taking into
341 account their modal proportions. The distribution of trace elements between solid and
342 melt in high-silica systems is imprecise, and therefore it is not always easy to select the
343 partition coefficients. In addition, there is often an important variation in the results
344 depending on the chosen Kd. For this work, some of the partition coefficients employed
345 in trace element modelling (fractional crystallization) (Table 5) have been used
346 previously by Jolliff et al. (1992) in their study of the petrogenetic relationships
347 between pegmatites and granites in the Black Hills (Dakota, USA); and by Roda-

348 Robles, 1993 and Vieira, 2010, to determine the relationships between granites and
349 aplite-pegmatites from the Fregeneda-Almendra field, located to the north of the Tres
350 Arroyos area, and also belonging to the Central Iberian Zone. Partition coefficients for
351 biotite have been compiled by Icenhower and London (1995) (Table 5).

352 The concentrations in Ba, Rb and Li of melts formed by different degrees of
353 fractional crystallization of a parent magma with the composition of the Nisa-
354 Alburquerque granite are plotted in Fig. 6. As Ba behaves as a compatible element in
355 this system, its concentration decreases in the residual melt with fractionation, whereas
356 Rb and Li, incompatible with most of the granite forming minerals, show an important
357 increase in the melts as fractional crystallization proceeds. A plot of the results of the
358 modelling together with the data of bulk-composition for the different lithologies may
359 be seen in Fig 6.
360
361 **5. Discussion**
362
363 *5.1. Geochemical evolution of quartz from Tres Arroyos*
364
365 Quartz crystallized during all the stages of magmatic/pegmatitic evolution of the
366 Tres Arroyos area, appearing in all the facies in this system. This makes quartz
367 especially suitable to evaluate the fractionation mechanisms and crystallization
368 processes that led to the different types of aplite-pegmatites occurring there, as it has
369 been done in a considerable number of cases with the chemistry of other rock-forming
370 minerals such as micas and/or K-feldspar (e.g., Roda et al., 1995; Foord et al., 1995;
371 Roda-Robles et al., 2006; Vieira et al., 2011; Martins et al., 2012).

372 The chemical composition of quartz from primitive granites is usually quite
373 homogeneous, in contrast to the quartz associated with highly fractionated granites and
374 pegmatites that uses to contain several populations of quartz with different trace
375 element contents (Larsen et al., 2004; Breiter and Müller, 2009; Müller et al., 2010).
376 However, despite of the highly fractionated nature of some of the magmatic facies
377 occurring in Tres Arroyos, according to the textural study under the microscope and to
378 the SEM-CL images (Fig. 3), all the quartz crystals in each facies crystallized primarily
379 from magmatic or pegmatitic melts, and nearly no subsolidus or hydrothermal
380 overprints affected this mineral.
381 Overall, quartz associated with the different magmatic facies from the Tres Arroyos
382 granite-pegmatite system is relatively rich in trace elements (mainly those behaving
383 incompatibly in the quartz structure, such as Al, Li, Ge, B and P), as it is the case of
384 other fractionated granites and pegmatites (e.g., Jacamon and Larsen, 2009; Breiter and
385 Müller, 2009; Müller et al., 2010; Beurlen et al., 2011; Drivenes et al., 2016) compared
386 with chemically more primitive granites and pegmatites, which commonly show much
387 lower contents in those elements (e.g., Larsen et al., 2004; Müller et al., 2008). Quartz
388 from the monzogranitic facies contains high Al values, lower values in the barren and
389 intermediate aplite-pegmatites, and the highest values are related to the Li-rich aplite-
390 pegmatites (Fig. 5a, b). Therefore, there is not a continuous increasing trend in the Al
391 content in quartz from the monzogranite, through the intermediate facies, up to the most
392 fractionated Li-rich aplite-pegmatites. When plotted Al versus Ti, which behaves as a
393 compatible element in quartz and, hence, decreases with decreasing temperature (Wark
394 and Watson, 2006), a “C”-shape trend is observed, with a positive Al-Ti correlation for
395 the highest Ti contents and a negative or no correlation for the lowest Ti values (Figs.
396 4a and 7). A quite similar trend has been already shown by Müller et al. (2002), Breiter

and Müller (2009) and Breiter et al. (2013) for the highly peraluminous P-rich granite suite of Podlesí, in the Saxothuringian Zone of the Bohemian Massif (Fig. 10), which is a Variscan granitic system with many similarities to that of the Tres Arroyos area (Roda-Robles et al., under review). Also in the Variscan Rozvadov S-type pluton from the Bohemian Massif (Breiter et al., 2013) and in the Land´s End granite in the Variscan Cornubian Batholith (Drivenes et al., 2016), positive Ti-Al correlations for the highest Ti contents in quartz are observed. Evidence for a single fractionation path starting from the Nisa-Alburquerque monzogranite is supported by the: (i) field relationships, (ii) results of the geochemical modelling (Fig. 6), (iii) continuous decrease in the Ti contents (Figs. 4a, c; 5d), and (iv) continuous increase of the Ge/Ti and Al/Ti ratios in quartz, the marginal granitic facies, the barren and intermediate aplite-pegmatites, and the Li-rich aplite-pegmatites (Fig. 4d, e). However, the Al content in quartz shows a more complex trend, which could be related to different factors. Some authors have proposed that an increase in the aluminium saturation index of the melt could increase the Al contents in quartz (Jacamon and Larsen, 2009). Nevertheless, the peraluminosity of the monzogranite in Tres Arroyos (and the Al content) is lower than that of the marginal granitic facies and of the barren and intermediate aplite-pegmatites, whereas its Al content in quartz is higher (Fig. 5). Only in the case of the most fractionated aplite-pegmatites (Li-rich dykes), the highest peraluminosity corresponds to the highest Al content in quartz. The depolymerization of alumina-silica complexes caused by high H_2O (Mysen 1987; Müller et al., 2000; Larsen et al., 2004; Breiter and Müller, 2009; Drivenes et al., 2016) or F (London, 1992; Breiter et al., 2013) contents in the parental magmas has been also suggested as a cause of an increase in the Al content in quartz. In the case of Tres Arroyos, according to bulk-rock chemical data, the amount of F was higher in the marginal granite and in the barren and intermediate aplite-pegmatites than

422 in the monzogranite; i.e., the higher F concentration in the melt is not reflected in a
423 higher Al content in quartz in those cases. Regarding the H_2O content of the melts, a
424 priori the water activity in residual late fractionates of granitic melts is supposed to be
425 higher than that of the parental magma. However, micas, the main OH-bearing mineral
426 in the barren and intermediate aplite-pegmatites from Tres Arroyos, are fairly scarce in
427 these rocks. Taking into account that the aplite-pegmatite dykes are supposed to have
428 crystallized in open fractures at relatively low pressures, we consider it feasible that the
429 crystallization of the pegmatitic melts in a relatively shallow, open system, allowed the
430 exsolution of a water-rich fluid phase that separated from the melt, lowering its water
431 content and, hence, preventing the incorporation of Al in the quartz (Larsen and
432 Jacamon, 2009). This did not happen during the crystallization of the monzogranite,
433 where micas are abundant and crystallization mainly proceeded under closed system
434 conditions and over 4 wt.% H_2O in the melt (González-Menéndez, 1998). Nevertheless
435 the scenario for the crystallization of the barren and intermediate aplite-pegmatites, with
436 an undercooled melt due to the sudden loss of H_2O and volatiles, crystallizing at
437 shallow emplacement levels, has been proposed to be suitable for a high growth rate in
438 quartz that would result in disequilibrium growth that may allow the uptake of Al and
439 other impurities into the quartz lattice (Pankrath, 1988; Merino et al., 1989). In this
440 sense, experimental data have shown that growth rate affects Ti and Al contents in
441 quartz (Huang and Audétat, 2012). Moreover, differences in the crystal structure of
442 alpha and beta quartz have been experimentally demonstrated to influence the capability
443 of quartz to incorporate Al and Li, favoured in the high-quartz (Frigo et al., 2016). In
444 such case, comparisons between beta quartz, the most likely primary quartz crystallized
445 in the monzogranitic facies (T of crystallization: 583°-652°C by applying the Ti-in
446 biotite geothermomether (Henry, 2005); 567-666°C by applying the TitaniQ

447 geothermometer (Thomas et al., 2010), assuming the system is saturated in ilmenite and
448 the Ti activity is in the range 0.5-1 (Ghent and Stout, 1984); final T of crystallization
449 close to 650°C according to the mineral paragenesis (González-Menéndez, 1998)); and
450 alpha quartz, presumably the primary silica polymorph crystallized in the marginal
451 granite (T of crystallization: 514-578°C by applying the Ti-in biotite geothermomether
452 (Henry, 2005)). All these facts suggest that, most probably, Al content in quartz
453 depends on different competing factors, which makes it much more difficult to
454 understand its variations during crystallization and fractionation.

455 After Al, Ti is the most abundant trace element in quartz associated with the
456 monzogranite (Fig. 4a, c, Table 3). There is an important decrease from this to the
457 quartz occurring in the marginal granitic facies; whereas Ti decreases gradually from
458 this facies, through the barren and intermediate aplite-pegmatites; with the lowest
459 values in the quartz from the Li-rich aplite-pegmatites (Fig. 4a, c, Table 3). Titanium
460 has been used as an indicator of temperature: high Ti contents are related to deep
461 magma reservoirs (Schrön et al., 1988), whereas a decreasing Ti concentration is
462 correlated to a lower crystallization temperature (Wark and Watson, 2006). Even if the
463 lack of Ti saturation in the studied aplite-pegmatites (no rutile in equilibrium with
464 quartz has been observed) prevents the use of the Ti-in quartz geothermometer (Huang
465 and Audétat, 2012), there is a clear descending trend in the Ti content in quartz during
466 fractionation in the Tres Arroyos granite-pegmatite system. Overall there is a good
467 positive correlation between the Ti content in quartz and the Ti concentration in the
468 hosting rock (Fig. 5). The marked decrease in Ti in the quartz from the monzogranite to
469 that from the marginal granitic facies may indicate a change in the conditions of
470 crystallization, with the transition from a granitic to a pegmatitic regime; or well, it
471 could respond to the crystallization of ilmenite in the monzogranite, much more

abundant than in the marginal granitic facies, which could buffer the Ti content in the residual melt.

The studied quartz is significantly enriched in Li compared to previous quartz studies owning to the fact that the Tres Arroyos suite is a Li enriched system. Thus, quartz from the monzogranite facies from Tres Arroyos is slightly enriched in this element when compared to other European granites, such as the granites from the Bohemian Massif, with the exception of the Nedjeck pluton (Breiter et al., 2013; Breiter and Müller, 2009); whereas similar Li-contents are described for the Land´s End Pluton in Cornwall (Drivenes et al., 2016). As it happens with the trend for the Al contents in quartz, the Li concentration is lower in the marginal granitic facies and in the barren and intermediate aplite-pegmatites, than in the monzogranite, with a final increase in the quartz from the Li-rich aplite-pegmatites (Fig. 4b, Table 3). Therefore, Li contents are strongly correlated with Al contents in quartz, with Li/Al atomic proportions close to 0.65 (Fig. 4b). The good correlation between Al and Li accounts for the substitution $Si^{4+} \Leftrightarrow Al^{3+} + Li^{+}$, where every atom of interstitial Li^{+} is counterbalancing one Al^{3+} atom replacing one Si^{4+} in the quartz structure. The introduction of other cations, such as K^{+}, Na^{+} and P^{5+} besides Li^{+}, and of Fe^{3+} and B^{3+} besides Al^{3+}, could have also operated in the quartz in some extent. Nevertheless, taking into account the general low concentrations of those elements in most of the analyzed quartz, the amount of Al that was not balanced by Li was most likely charge compensated by H^{+}, as proposed by Müller and Koch-Müller, (2009), Breiter et al. (2013), and, Baron et al. (2015). As it happens with Al, in general there is no correlation between Li contents in the quartz and in the bulk rock (Fig. 5), as it was described for some pegmatites from the Bohemian Massif by Breiter et al. (2014). Lithium contents in quartz have been related to the peraluminosity of the melt (Jacamon and Larsen, 2009), as well as to the fractionation degree and coexisting

497 Li-bearing minerals (Breiter et al., 2013, 2014). However, none of these reasons seems
498 easy to apply in this case, as discussed above for Al. Taking into account the good Al/Li
499 correlation, we consider that the Li proportion in the quartz is most likely conditioned
500 by the Al incorporation into quartz lattices, at least for low and intermediate Li
501 concentrations in the bulk rock.

502 Germanium is another trace element of quartz that reflects the degree of melt
503 differentiation. According to Jacamon and Larsen, (2009), the Ge/Ti ratio in quartz
504 usually increases with fractionation. Such is the case in the Tres Arroyos system, where
505 Ge concentration increases from the monzogranite, through the barren aplite-
506 pegmatites, up to the most fractionated dykes (Table 3, Fig. 4c). When compared to the
507 Ge content in quartz and in the whole rock, there is certain correlation, mainly for the
508 poorest (monzogranite) and richest (Li-rich aplite-pegmatites) ones (Fig. 5).

509 The remaining trace elements (B, Fe, K, P, Na) show low contents for most of the
510 analyzed samples. The most abundant of those is K, mainly in quartz associated with
511 the monzogranite and the Li-rich pegmatites; showing a similar correlation with Al as
512 Li ($Si \Leftrightarrow Al^{3+} + K^{+}$). Phosphorus occurs also in appreciable amounts, in the ranges 1-5,
513 2 -3, 0-8, 1-9, 0-8 for the monzogranite, marginal granite, barren, intermediate and Li-
514 rich aplite-pegmatites respectively. No correlation has been observed between Al and P,
515 which means that a supposed incorporation of P via the berlinite substitution ($2Si^{4+} \Leftrightarrow$
516 $Al^{3+} + P^{5+}$) was not significant (Maschmeyer and Lehmann, 1983). Boron may also
517 appear in measurable concentrations, with an overall gradual increase with fractionation
518 from monzogranite to the Li-rich aplite-pegmatites (Table 3, Fig. 4e). Tourmaline is the
519 only B-bearing mineral occurring in these rocks, and occurs in the marginal granitic
520 facies and barren pegmatites. The B content in quartz from these lithologies does not
521 seem to be significantly affected by the crystallization of tourmaline, as it fits in the

522 increasing trend from monzogranite toward more fractionated facies. The addition of
523 K^+, Na^+ and P^{5+} to Li^+, and of Fe^{3+} and B^{3+} to Al^{3+}, in the plot of Al versus Li (Fig. 4b),
524 increases just slightly the degree of correlation, diminishing insignificantly the deviation
525 from the 1:1 atomic proportion vector (Fig. 4f). This indicates that the substitutions
526 Si⇔ Al^{3+} + K^+, Si⇔ Al^{3+} + Na^+ and the same ones with B^{3+} or Fe^{3+} instead of Al^{3+},
527 could have operated in the quartz but in a very limited way. The extremely low Fe and
528 Mn contents in the quartz from the aplite-pegmatites (< 1 $\mu g g^{-1}$) could indicate that the
529 impact of meteoric fluids during quartz primary crystallization was negligible, opposite
530 to that observed in the stockscheider of Podlesí (Bohemian Massif) (Breiter and Müller,
531 2009), with significant mineral, chemical and textural similarities to those of the aplite-
532 pegmatites from Tres Arroyos (Roda-Robles et al., under review).
533
534 *5.2. Fractionation trends and internal evolution of the aplite-pegmatite dykes*
535
536 Taking Ti as a compatible element to get inside the quartz structure, and Al and Ge
537 as incompatible ones, the Al/Ti and Ge/Ti ratios have been also used to illustrate the
538 fractionation trends of different plutons (Breiter et al., 2012; 2013; Jacamon and Larsen
539 2009; Drivenes et al., 2016). As stated above, in the quartz from Tres Arroyos the two
540 ratios increase with fractionation, with a strong positive correlation among them (Fig.
541 4d, e), also observed for the whole rock data (Fig. 5). According to these data, the
542 monzogranite is the less fractionated lithology. The marginal granitic facies and the
543 barren aplite-pegmatites show a higher evolution degree, followed by the intermediate
544 aplite-pegmatites. Finally, the highest fractionation level is attained by the Li-rich
545 aplite-pegmatites.

546 A quite similar trend is also obtained by the geochemical modelling applying
547 Rayleigh equations to the Li, Rb and Ba bulk contents of the Alburquerque
548 monzogranite, and comparing the results to the bulk contents of the rest of lithologies in
549 the Tres Arroyos system (Fig. 6). According to the data, the different lithologies may be
550 explained by a single crystallization path that well could start from a composition
551 similar to that of the Nisa-Alburquerque monzogranitic facies. At fractionation degrees
552 of ≈ 50% the marginal granitic facies could crystallize; whereas extreme degrees of
553 fractionation (≈ 99%) would be necessary to obtain the concentrations in Ba, Li and Rb
554 observed in the lepidolite-rich aplite-pegmatites. Intermediate degrees of fractionation
555 are needed for the barren and intermediate aplite-pegmatites (Fig. 6). Deviations from
556 the ideal fractionation trends are observed for some of the samples, mainly those from
557 the albite-richest bodies (Fig. 6). Such deviations may be attributed to different reasons:
558 firstly, it could be related to the representativeness of the analyzed samples, as the
559 strong heterogeneity of these rocks makes it often difficult to obtain a sample
560 representative of the whole-rock composition; secondly, the mineral association of the
561 albite-richest rocks is not probably the most suitable to make a modelling for the Ba, Li
562 and Rb, as these elements are usually hosted in micas and K-feldspar, whereas albite
563 shows much lower values; and, thirdly, in some of these dykes metasomatic processes,
564 mainly including albitization, seem to be locally important, which would most probably
565 change the primary Ba, Rb and Li concentrations in those aplite-pegmatites.
566 Accordingly, fractional crystallization was an important mechanism that well could
567 explain the chemical and mineral variations observed for the different facies occurring
568 in the Tres Arroyos granite-pegmatite system and the extreme Li-F-enrichment in the
569 most evolved aplite-pegmatites. Crystal fractionation is often also reflected inside single
570 pegmatitic bodies all over the world, where an internal zoning is developed during

571 crystallization, usually from the borders inward with the most fractionated facies
572 occurring in the core margin and core zone, witnessing the internal evolution of the melt
573 (e.g., London, 2008, Roda-Robles et al., 2012b; Roda-Robles et al., 2015). Such is not
574 the case of the aplite-pegmatites from Tres Arroyos, which do not present internal
575 zoning nor quartz cores. However, the presence of comb textured feldspars and quartz
576 crystals, growing perpendicularly to the pegmatite contacts and increasing in width in
577 the direction of the core of the bodies; as well as the frequent occurrence of layering
578 disposed parallel to the margins of the dykes, indicate that crystallization in the Tres
579 Arroyos aplite-pegmatite dykes also proceeded mainly from the borders inward. Studies
580 on the variation of the trace elements contents in quartz during the crystallization of
581 single pegmatites are scarce: e.g. strong variations have been observed in some LCT
582 pegmatites from the Borborema Pegmatite Province (Beurlen et al., 2011); similar
583 evolutionary trends from fractioned granites to LCT pegmatites are described in the
584 Bohemian Massif, (Breiter et al., 2014); noticeable variations are also described for the
585 NYF pegmatites in Evje-Iveland (Müller et al., 2015). In contrast, almost no variation is
586 found in quartz chemistry across the internally zoned abyssal pegmatites from Froland
587 (Müller et al., 2015). In order to check a possible internal fractionation in the aplite-
588 pegmatites from Tres Arroyos, quartz from different layers was analyzed. According to
589 the obtained data, no variation in the contents of trace elements is noticed from the
590 contacts inwards the dykes. This, together with the lack of internal zoning inside the
591 aplite-pegmatites, where, for example, in the Li-rich dykes the Li-rich micas crystallize
592 across the whole aplite-pegmatite body, indicate that during the crystallization of the
593 aplite-pegmatites, fractionation of the melts was negligible. The distribution of the most
594 fractionated aplite-pegmatites occurring farthest from the monzogranite (Fig. 1)
595 suggests a previous vertical chemical zonation of the melt within the source pluton, as it

596 has been indicated for the Fregeneda-Almendra field, occurring to the north of Tres
597 Arroyos, also in the CIZ, and in some Li-rich leucogranitic cupolas occurring in the
598 region (Roda-Robles et al., 2012a; Roda-Robles et al., 2016, Roda-Robles et al., under
599 review). Such compositional zoning in the melt would have developed in the magma
600 chamber before the granitic system opened and the melt intruded the fractures where it
601 finally crystallized. The greater enrichment in Li, F, and probably also H_2O at the top of
602 the magma chamber would notably reduce the viscosity of the most fractionated melts
603 (Dingwell et al., 1996), and would also lower the liquidus temperature, enhancing its
604 mobility. That most fractionated portion of melt in the upper part of the magma
605 chamber would escape first and move further. The aplite-pegmatite dykes from Tres
606 Arroyos are relatively thin, with thicknesses under 7 m. The temperature of the hosting
607 metasediments at epizonal emplacement levels (350-400ºC) was presumably
608 significantly lower than that of the intruded melt (over 500°C according to the presence
609 of monoclinic feldspar in all the aplite-pegmatite dykes), which would cause an
610 important undercooling of the melt and the increase of its solidus temperature,
611 reinforced by the likely exsolution of a fluid phase from the pegmatitic melt, mainly due
612 to the drop of pressure. Pegmatites crystallizing in similar scenarios have been modelled
613 by Webber et al. (1999) in order to calculate their crystallization time, obtaining very
614 short periods, in the order of days to weeks. Therefore, all these evidences suggest that
615 once intruded into the fractures, melts should crystallize very quickly, preventing the
616 internal fractionation of the aplite-pegmatite. It has also been suggested that low Rb
617 contents in quartz, as it is the case, correspond to rapid crystallization at low pressures,
618 after melt emplacement (Breiter et al., 2013). Therefore, the lack of variation in the
619 trace element contents in quartz from different layers reflects the lack of internal zoning
620 inside individual dykes, probably due to the rapid crystallization of the melt.

621

622

623 **6. Conclusions**

624

625 Taking into account the textural and chemical variations observed in the studied
626 quartz, together with the geochemical modelling on whole-rock data, the following
627 conclusions can be summarized:

628

629 1) Quartz from the highly evolved Tres Arroyos granite-pegmatite system
630 crystallized primarily from magmatic or pegmatitic melts, with no evident
631 subsolidus or hydrothermal overprint.
632 2) Aluminium, Li, Ti, and Ge are the main trace elements in the studied quartz,
633 with different concentrations depending on the facies: the highest Al, Li and
634 Ge, and the lowest Ti being associated with the quartz from the most
635 fractionated aplite-pegmatites (Li-rich), and the highest Ti values with the
636 monzogranite.
637 3) Continuous trends for the main trace elements are observed for the quartz
638 from the monzogranite, through the marginal granitic facies, the barren and
639 intermediate aplite-pegmatites, up to the most evolved Li-rich dykes.
640 Titanium contents decrease in that sense, i.e. with descending temperature;
641 whereas the inflexion observed in the Al and Li values suggests the influence
642 of different competing factors (e.g., chemical composition and content in
643 water of the melt, P and T conditions, rate of crystallization, quartz structure).
644 4) The good correlation between Al and Li, suggests that the main substitution
645 mechanism for the inclusion of these two elements in the quartz was: $Si^{4+} \Leftrightarrow$

Al^{3+} + Li^{+}. The important deviation of the Li/Al rate below the 1:1 atomic proportion vector, suggests that the remaining Al was equilibrated by H^{+} ions.

5) A continuous fractionation trend from the monzogranite up to the most fractionated pegmatites is evidenced from the trace element contents in quartz and from the geochemical modelling (Rayleigh fractional crystallization): the granitic melt should fractionate over 50% to obtain the composition of the marginal granitic facies and the barren aplite-pegmatites, and over ≈ 99% for the most fractionated Li-rich dykes.

6) The negligible and erratic variations of the trace elements contents of quartz in the different layers inside the aplite-pegmatites suggest the lack of internal fractionation inside the dykes, probably as a consequence of a rapid crystallization from highly undercooled melts, in contact with a colder hosting-rock.

Acknowledgements

Comments and sugestions made by Rune B. Larsen and Karel Breiter and the Editor, Nelson Eby, have considerably increased the quality of the manusccript The authors are indebted to the mining company IMERYS, which has always facilitated access to the Tres Arroyos quarry. This research has been supported financially by the Spanish Ministerio de Economía y Competitividad (Project CGL2012- 31356, with ERDF funds; Project CGL2016-78796). Also the University of the Basque Country-UPV/EHU contributed economically with the grant GIU/1216. Idoia Garate-Olave has been financed by Gobierno Vasco/Eusko Jaurlaritza.

671

672 **References**

673 Baron, M.A., Stalder, R., Konzett, J. and Hauzenberger, C.A., 2014. OH-point defects
674 in quartz in B- and Li-bearing systems and their application to pegmatites.
675 Physics and Chemistry of Minerals 42(1), 53-62.
676 Beurlen, H., Müller, A., Silva, D. and Da Silva, M.R.R., 2011. Petrogenetic significance
677 of LA-ICP-MS trace-element data on quartz from the Borborema Pegmatite
678 Province, northeast Brazil. Mineralogical Magazine 75(5), 2703-2719.
679 Breiter, K., Ackerman, L., Ďurišová, J., Svojtka, M. and Novák, M., 2014. Trace
680 element composition of quartz from different types of pegmatites: A case study
681 from the Moldanubian Zone of the Bohemian Massif (Czech Republic).
682 Mineralogical Magazine 78(3), 703-722.
683 Breiter, K., Ackerman, L., Svojtka, M. and Müller, A., 2013. Behavior of trace elements
684 in quartz from plutons of different geochemical signature: A case study from the
685 Bohemian Massif, Czech Republic. Lithos 175-176, 54-67.
686 Breiter, K. and Müller, A., 2009. Evolution of rare-metal granitic magmas documented
687 by quartz chemistry. European Journal of Mineralogy 21(2), 335-346.
688 Breiter, K., Svojtka, M., Ackerman, L. and Švecová, K., 2012. Trace element
689 composition of quartz from the Variscan Altenberg–Teplice caldera (Krušné
690 hory/Erzgebirge Mts, Czech Republic/Germany): Insights into the volcano-
691 plutonic complex evolution. Chemical Geology 326-327, 36-50.
692 Černý, P., 1989. Characteristics of pegmatite deposits of tantalum. En : Möller P.,
693 Černý P., Saupé, F. (eds): Lanthanides, Tantalum and Niobium. SGA Special
694 Publication 7, 192-236.

695 Černý, P. and Burt, D.M., 1984. Paragenesis, crystallochemical characteristics, and
696 geochemical evolution of micas in granitic pegmatites. In Bailey S.W. Ed.,
697 Micas. Mineralogical Society of America., Review in Mineralalogy 13, 257-298.
698 Deans, J.R.L., 2010. Trace element and calculated temperature cariation in quartz and
699 titanite in the 36 Ma Harrison Pass pluton, Ruby Mountains NE Nevada. Phd
700 Thesis, Texas Tech. University.
701 Dennen, W.H., 1966. Stoichiometric substitution in natural quartz. Geochimica et
702 Cosmochimica Acta 30, 1235-1241.
703 Dingwell, D.B., Hess, K.U. and Knoche, R., 1996. Granite and granitic pegmatite melts:
704 Volumes and viscosities. Transactions Of The Royal Society Of Edinburgh-
705 Earth Sciences 87, 65-72.
706 Drivenes, K., Larsen, R.B., Müller, A. and Sørensen, B.E., 2016. Crystallization and
707 uplift path of late Variscan granites evidenced by quartz chemistry and fluid
708 inclusions: Example from the Land's End granite, SW England. Lithos 252-253,
709 57-75.
710 Foord, E.E., Černý, P., Jackson, L.L., Sherman, D.M. and Eby, R.K., 1995.
711 Mineralogical and Geochemical Evolution of Micas from Miarolitic Pegmatites
712 of the Anorogenic Pikes-Peak Batholith, Colorado. Mineralogy and Petrology
713 55(1-3), 1-26.
714 Frigo, C., Stalder, R. and Hauzenberger, C.A., 2016. OH defects in quartz in granitic
715 systems doped with spodumene, tourmaline and/or apatite: experimental
716 investigations at 5–20 kbar. Physics and Chemistry of Minerals 43(10), 717-729.
717 Gallego-Garrido, M., 1992. Las mineralizaciones de Li asociadas a magmatismo ácido
718 en Extremadura y su encuadre en la Zona Centro-Ibérica. PhD Thesis,
719 Universidad Complutense de Madrid, Spain, 323 pp.

720 Ghent, E.D. and Stout, M.Z., 1984. TiO2 activity in metamorphosed pelitic and basic
721 rocks: principales and appications to methamorphism in southeastern Canadian
722 Cordillera. Contribution of Mineralogy and Petrology 86, 248-255.
723 González-Menéndez, L., 1998. Petrología y Geoquímica del Batolito Granítico de Nisa-
724 Alburquerque (Alto Alentejo, Portugal; Extremadura, España). PhD thesis. Phd
725 Thesis, Universidad de Granada, 223 pp.
726 González-Menéndez, L.G., Azor, A., Ordóñez, A.R. and Sánchez-Almazo, I., 2010. The
727 metamorphic aureole of the Nisa-Alburquerque batholith (SW Iberia):
728 implications for deep structure and emplacement mode. International Journal of
729 Earth Sciences 100(7), 1533-1550.
730 Götze, J., Plotze, M., Graupner, T., Hallbauer, D.K. and Bray, C.J., 2004. Trace element
731 incorporation into quartz: A combined study by ICP-MS, electron spin
732 resonance, cathodoluminescence, capillary ion analysis, and gas
733 chromatography. Geochimica Et Cosmochimica Acta 68(18), 3741-3759.
734 Götze, J., Plotze, M. and Habermann, D., 2001. Origin, spectral characteristics and
735 practical applications of the cathodolumimescence (CL) of quartz - a review.
736 Mineralogy and Petrology 71(3-4), 225-250.
737 Götze, J., Plotze, M. and Trautmann, T., 2005. Structure and luminescence
738 characteristics of quartz from pegmatites. American Mineralogist 90(1), 13-21.
739 Henry, D.J., Guidotti, C.V. and Thompson, J.A., 2005. The Ti-saturation surface for
740 low-to-medium pressure metapelitic biotites: Implications for geothermometry
741 and Ti-substitution mechanisms. American Mineralogist 90, 316-328.
742 Huang, R. and Audétat, A., 2012. The titanium-in-quartz (TitaniQ) thermobarometer: A
743 critical examination and recalibration. Geochimica et Cosmochimica Acta 84,
744 75-89.

745 Icenhower, J. and London, D., 1995. An experimental study of element partitioning
746 among biotite, muscovite, and coexisting peraluminous silicic melt at 200 MPa
747 (H2O). American Mineralogist 80(11-12), 1229-1251.
748 Jacamon, F. and Larsen, R.B., 2009. Trace element evolution of quartz in the
749 charnockitic Kleivan granite, SW-Norway: The Ge/Ti ratio of quartz as an index
750 of igneous differentiation. Lithos 107(3-4), 281-291.
751 Jochum, K.P., Weis, U., Stoll, B., Kuzmin, D., Yang, Q., Raczek, I., Jacob, D.E.,
752 Stracke, A., Birbaum, K., Frick, D.A., Günther, D. and Enzweiler, J, Aguilar
753 Tomás M., 2011. Determination of reference values for NIST SRM 610-617
754 glasses following ISO guidelines. Geostandards and Geoanalytical Research
755 35(397-429), 397-429.
756 Jolliff, B.L., Papike, J.J. and Shearer, C.K., 1992. Petrogenetic relationships between
757 pegmatite and granite based on geochemistry of muscovite in pegmatite wall
758 zones, Black Hills, South Dakota, USA. Geochimica Et Cosmochimica Acta 56,
759 1915-1939.
760 Larsen, R.B., 2002. The distribution of rare-earth elements in K-feldspar as an indicator
761 of petrogenetic processes in granitic pegmatites: examples from two pegmatite
762 fields in southern Norway. Canadian Mineralogist 40, 137-151.
763 Larsen, R.B., Henderson, I., Ihlen, P.M. and Jacamon, F., 2004. Distribution and
764 petrogenetic behaviour of trace elements in granitic pegmatite quartz from South
765 Norway. Contributions to Mineralogy and Petrology 147(5), 615-628.
766 London, D., 1992. The application of experimental petrology to the genesis and
767 crystallization of granitic pegmatites Canadian Mineralogist 30, 499-540.
768 London, D., 2008. Pegmatites. The Canadian Mineralogist, Special Publication nº 10,
769 347.

770 Marchal, K.L., Simmons, W.B., Falster, A.U., Webber, K.L. and Roda-Robles, E.,
771 2014. Geochemistry, Mineralogy, And Evolution Of Li-Al Micas And Feldspars
772 From The Mount Mica Pegmatite, Maine, USA. The Canadian Mineralogist
773 52(2), 221-233.
774 Martins, T., Roda-Robles, E., Lima, A. and de Parseval, P., 2012. Geochemistry and
775 Evolution of Micas in the Barroso-Alvao Pegmatite Field, Northern Portugal.
776 The Canadian Mineralogist 50(4), 1117-1129.
777 Maschmeyer, D. and Lehmann, G., 1983. A trapped-hole center causing rose coloration
778 of natural quartz. Zeitschrift für Kristallographie 163, 181-196.
779 Merino, E., Harvey, C. and Murray, H.H., 1989. Aqueous-chemical control of the
780 tetrahedral-aluminum content of quartz, halloysite and other low-temperature
781 silicates. Clays and Clay Minerals 37, 135-142.
782 Müller, A., Ihlen, P.M. and Kronz, A., 2008. Quartz chemistry in polygeneration
783 Sveconorwegian pegmatites, Froland, Norway. European Journal of Mineralogy
784 20(4), 447-463.
785 Müller, A. et al., 2015. The Chemistry of Quartz in Granitic Pegmatites of Southern
786 Norway: Petrogenetic and Economic Implications. Economic Geology 110,
787 1737-1757.
788 Müller, A. and Koch-Müller, M., 2009. Hydrogen speciation and trace element contents
789 of igneous, hydrothermal and metamorphic quartz from Norway. Mineralogical
790 Magazine 73(4), 569-583.
791 Müller, A., Seltmann, R. and Behr, H.J., 2000. Application of cathodoluminescence to
792 magmatic quartz in a tin granite case study from the Schellerhau Granite
793 Complex, Eastern Erzgebirge, Germany. Mineralium Deposita 35, 169-189.

794 Müller, A., van den Kerkhof, A.M., Behr, H.-J., Kronz, A. and Koch-Müller, M., 2010.
795 The evolution of late-Hercynian granites and rhyolites documented by quartz – a
796 review. Earth and Environmental Science Transactions of the Royal Society of
797 Edinburgh 100(1-2), 185-204.
798 Müller, A., Wiedenbeck, M., van den Kerkhof, A.M., Kronz, A. and Simon, K., 2003.
799 Trace elements in quartz – a combined electron microprobe, secondary ion mass
800 spectrometry, laser-ablation ICP-MS, and cathodoluminescence study. European
801 Journal of Mineralogy 15(4), 747-763.
802 Müller, A., Williamson, B.J. and Smith, M., 2005. Origin of quartz cores in tourmaline
803 from Roche Rock, SW England. Mineralogical Magazine 69(4), 381-401.
804 Mysen, B.O., 1987. Magmatic silicate melts: Relations between bulk composition,
805 structure and propertie. In: B.O. Mysen (Editor), Magmatic processes:
806 Physiocochemical principle. The Geochemical Society Special Publication No.
807 1. Lancaster Press, Inc., Pennsylvania, pp. 375-399.
808 Neumann, H., Mead, J. and Vitaliano, C.J., 1954. Trace elemen variation during
809 fractional crystallization as calculated from the distribution law. Geochimica e
810 Cosmochimica Acta 6, 90-99.
811 Norton, J.J., 1973. Lithium, cesium and rubidium - the rare alkali metal. United States
812 mineral resources: U.S. Geological Survey Professional Paper 820, 365-378.
813 Novak, M., Kadlec, T. and Gadas, P., 2013. Geological position, mineral assemblages
814 and contamination of granitic pegmatites in the Moldanubian Zone, Czech
815 Republic; examples from the Vlastejovice region. Journal of Geosciences 58(1),
816 21-47.

817 Pankrath, R., Spurenelementeinbau in Tief-Quarz als Funktion
818 derWachstumsbedingungen und Umpräigungen unter trockenen und
819 hydrothermalen Bedingunge. PhD Thesis, Ruhr-Univenität Bochum, Germany.
820 Perny, B., Eberhardt, P., Ramseyer, K., Mullis, J. and Pankrath, R., 1992.
821 Microdistribution of Al, Li, and Na in quartz: possible causes and correlation
822 with short-lived cathodoluminescence. American Mineralogist 77, 534-544.
823 Ramseyer, K., Baumann, J., Matter, A. and Mullis, J., 1988. Cathodoluminescence
824 colours of alpha-quartz. Mineralogical Magazine 52, 669-677.
825 Roda, E., Keller, P., Pesquera, A. and Fontan, F., 2007. Micas of the muscovite–
826 lepidolite series from Karibib pegmatites, Namibia. Mineralogical Magazine
827 71(1), 41-62.
828 Roda, E., Pesquera, A. and Velasco, F., 1995. Micas of the Muscovite-Lepidolite Series
829 from the Fregeneda Pegmatites (Salamanca, Spain). Mineralogy and Petrology
830 55(1-3), 145-157.
831 Roda-Robles, E., 1993. Distribución, características y petrogénesis de las pegmatitas de
832 La Fregeneda (Salamanca). PhD Thesis, Universidad del País Vasco, Spain, 199
833 pp.
834 Roda-Robles, E., Pesquera, A., Gil-Crespo, P. and Torres-Ruiz, J., 2012a. From granite
835 to highly evolved pegmatite: A case study of the Pinilla de Fermoselle granite–
836 pegmatite system (Zamora, Spain). Lithos 153, 192-207.
837 Roda-Robles, E., Pesquera, A., Gil-Crespo, P.P. and Torres-Ruiz, J., 2012b. The
838 Puentemocha beryl-phosphate granitic pegmatite, Salamanca, Spain: Internal
839 structure, petrography and mineralogy. Canadian Mineralogist 50(6), 1573-
840 1587.

841 Roda-Robles, E., Pesquera, A., Gil-Crespo, P.P., Torres-Ruiz, J. and De Parseval, P.,
842 2006. Mineralogy and geochemistry of micas from the Pinilla de Fermoselle
843 pegmatite (Zamora, Spain). European Journal Of Mineralogy 18(3), 369-377.
844 Roda-Robles, E. et al., 2016. Geology and mineralogy of Li mineralization in the
845 Central Iberian Zone (Spain and Portugal). Mineralogical Magazine 80(1), 103-
846 126.
847 Roda-Robles, E., Pesquera, A. and Velasco, F. (Editors), 1993. Mica and K-feldspar as
848 indicators of pegmatite evolution the Fregeneda area (Salamanca, Spain).
849 Current research in geology applied to ore deposits, Granada, 653-656 pp.
850 Roda-Robles, E. et al., 2015. Tourmaline as a petrogenetic monitor of the origin and
851 evolution of the Berry-Havey pegmatite (Maine, U.S.A.). American
852 Mineralogist 100, 95-109.
853 Roda-Robles, E. et al., Under review. Petrogenetic relationships among Variscan
854 granitoids and Li-(f-P)-rich aplite-pegmatotes in Central Iberian Zone:
855 geological and geochemical constraints and implications for the other regions
856 from the European Variscides. Earth-science Reviews.
857 Rusk, B., 2012. Cathodoluminiscent textures and trace elements in hydrothermal quartz.
858 Quartz: Deposits, Mineralogy and Analytics.
859 Rusk, B.G., Lowers, H.A. and Reed, M.H., 2008. Trace elements in hydrothermal
860 quartz: Relationships to cathodoluminescent textures and insights into vein
861 formation. Publicatoin of an organization other than U.S. Geological Survey
862 36(7), 547-550.
863 Schrön, W., Schmädicke, E., Thomas, R. and Schmidt, W., 1988. Geochemische
864 Untersuchungen an Pegmatitquarzen. Zeitschrift für Geologische
865 Wissenschaften 16, 229-244.

866 Shmakin, B.M., 1983. Geochemistry and origin of granitic pegmatite. Geochemistry
867 International 20, 1-8.
868 Simmons, W., Falster, A., Webber, K. and Roda-Robles, E., In press. Bulk composition
869 of mt. Mica pegmatite, Maine, USA: Implications for the origin of an LCT type
870 pegmatite by anatexis. The Canadian Mineralogist.
871 Simmons, W.B., Foord, E.E., Falster, A.U. and King, V.T., 1995. Evidence for an
872 anatectic origin of granitic pegmatites, western Maine, USA. Geol. Soc. Amer.
873 Annual Meeting., Abstr Programs 27, A411.
874 Simmons, W.B. and Webber, K.L., 2008. Pegmatite genesis: state of the art. European
875 Journal of Mineralogy 20(4), 421-438.
876 Sokolov, Y.M., 1982. Chapter 12 - Precambrian metamorphogenic pegmatites, The
877 Development Potential of Precambrian Mineral Deposits. Pergamon, pp. 157-
878 164.
879 Solá, A.R., Williams, I.S., Neiva, A.M.R. and Ribeiro, M.L., 2009. U–Th–Pb SHRIMP
880 ages and oxygen isotope composition of zircon from two contrasting late
881 Variscan granitoids, Nisa-Albuquerque batholith, SW Iberian Massif: Petrologic
882 and regional implications. Lithos 111(3-4), 156-167.
883 Sprunt, E.S., 1981. Causes of quartz cathodoluminescence colors. Scanning Electron
884 Microscopy. 525-535.
885 Stevens Kalceff, M.A., Phillips, M.R., Moon, A.R. and W, K., 2000.
886 Cathodoluminescence microcharacterization of silicon dioxide polymorphs.
887 Pagel M, Barbin V, Blanc P, Ohnenstetter D(eds) Cathodoluminescence in
888 geoscience, 193-224.
889 Stewart, D.B., 1978. Petrogenesis of lithium-rich pegmatites. American Mineralogist
890 63, 970-980.

Thomas, J.B. et al., 2010. TitaniQ under pressure: the effect of pressure and temperature on the solubility of Ti in quartz. Contributions to Mineralogy and Petrology 160(5), 743-759.

Vieira, R., 2010. Aplitopegmatitos com elementos raros da região entre Almendra (V. N. de Foz-Côa) e Barca d'Alba (Figueira de Castelo Rodrigo). Campo aplitopegmatítico da Fregeneda-Almendra. PhD Thesis, Universidade do Porto, Portugal, 275 pp.

Vieira, R., Roda-Robles, E., Pesquera, A. and Lima, A., 2011. Chemical variation and significance of micas from the Fregeneda-Almendra pegmatitic field (Central-Iberian Zone, Spain and Portugal). American Mineralogist 96(4), 637-645.

Wark, D.A. and Watson, E.B., 2006. TitaniQ: a titanium-in-quartz geothermometer. Contributions to Mineralogy and Petrology 152, 743-754.

Webber, K.L., Simmons, W.B., Falster, A.U. and Foord, E.E., 1999. Cooling rates and crystallization dynamics of shallow level pegmatite-aplite dikes, San Diego County, California. American Mineralogist 84(5-6), 708-717.

Figure caption

Fig. 1: Schematic geological map of the Central Iberian Zone (CIZ) and detailed map from the Tres Arroyos pegmatitic field (modified from Gallego-Garrido 1992). Locations of studied samples: 1) Barren aplite-pegmatites; 2) Intermediate aplite-pegmatites; 3) Layered intermediate aplite-pegmatites; 4) Li-rich aplite-pegmatites

Fig. 2: (a) Sample from an intermediate aplite-pegmatite showing a simple pattern layering, with alternating albite-rich layers with quartz-rich layers (b) hand sample from

916 a Li-rich dyke exhibiting a complex layering (for location of the samples see Figure 1).

917

918 Fig. 3: SEM-CL images from: (a) homogeneous quartz from the monzogranitic facies
919 showing little cracks; (b) quartz from intermediate aplite-pegmatite with a weakly-
920 contrasted growth zoning; (c) and (d) quartz from an intermediate and a Li-rich dyke
921 respectively, with intra and transgranular healed cracks (for location of the samples see
922 Figure 1).

923

924 Fig. 4: Plot of the trace elements contents in quartz: (a) Al *vs* Ti; (b) Al *vs* Li, the arrows
925 indicate Li/Al atomic ratios 1:1 and 1:2; (c) Ti *vs* Ge; (d) Al/Ti *vs* Ge/Ti; (e) Ge/Ti *vs* B;
926 (f) molar values of ΣAl + B + Fe *vs* Σ Li + K + Na + P, the arrows indicate
927 (Li+K+Na+P)/(Al+B+Fe) atomic rates 1:1 and 1:2.

928

929 Fig. 5: (a, b, c, d) Plots of Li, Ge, Al and Ti contents from whole rock *vs* trace element
930 contents from quartz analyses (e) Ge/Ti vs Al/Ti from bulk rock.

931

932 Fig. 6: Plot of (a) Li *vs* Ba, and (b) Rb *vs* Ba, for different bodies from Tres Arroyos
933 area, and the possible path of fractional crystallization of a parent magma with the
934 composition of the Nisa-Alburquerque monzogranite. Filled symbols represent our data,
935 empty symbols represent data from Gallego-Garrido, 1992, half-filled symbol
936 represents data from González-Menéndez, 1998.

937

938 Fig. 7: Variations in the Ti and Al contents in the different facies from the Tres Arroyos
939 system and comparison with quartz from other granitic and pegmatitic quartz
940 occurrences (data modified from (Breiter et al., 2013): Nejdek pluton (Breiter and

941 Müller, 2009), Central Moldanubian and Rozvadov (Breiter et al., 2013); Ruby
942 mountains granites (Deans, 2010); Norwegian Precambrian granites (Jacamon and
943 Larsen, 2009); and, Borborema pegmatites (Beurlen et al., 2011)).
944
945 Table 1: Mineralogy and petrography of the different facies from the Tres Arroyos
946 aplite-pegmatite-granite system.
947
948 Table 2: Detection limits of trace elements of LA-CP-MS analyses (in $\mu g g^{-1}$).
949
950 Table 3: Range of values of trace elements in quartz from the different granite and
951 pegmatite types, analyzed by LA-ICP-MS (all values given in $\mu g g^{-1}$).
952
953 Table 4: Average values and their standard deviation of trace element in quartz from
954 different layers from the three types of aplite-pegmatites, analyzed by LA-ICP-MS.
955
956 Table 5: Mineral modes from a representative monzogranite and partition coefficients
957 used in the modelling of fractional crystallization. For quartz, K-feldspar, plagioclase
958 and muscovite, data compiled by Jollif et al., 1992; for biotite, data compiled by
959 Icenhower and London, 1995.

39.25º

-7.08º

Rivera del Arconeo

CZ=Cantabrian Zone
WALZ=West Asturian-Leonese Zone
CIZ=Central Iberian Zone
GTMZ=Galicia Tras Os Montes Zone
OMZ=Ossa Morena Zone
SPZ=South Portuguese Zone

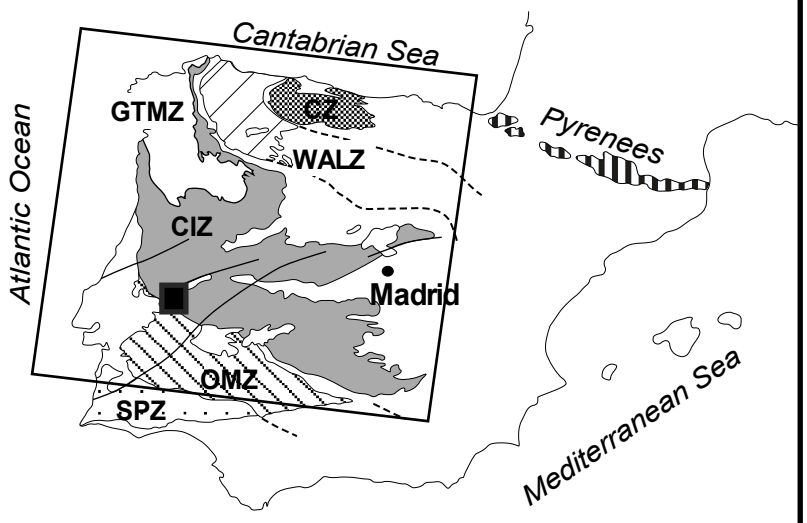

N

500m

Schist Metagreywacke Complex (SMC)
Monzogranite
Marginal granitic facies
Barren aplite-pegmatites
Intermediate aplite-pegmatites
Li-rich aplite-pegmatites
Li-rich aplite-pegmatites (not outcropping)
Dumps

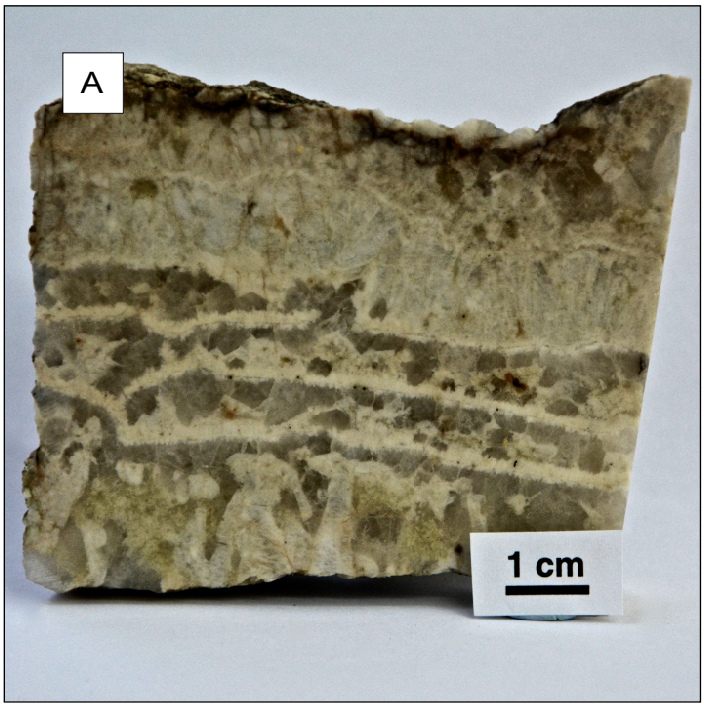
A
1 cm

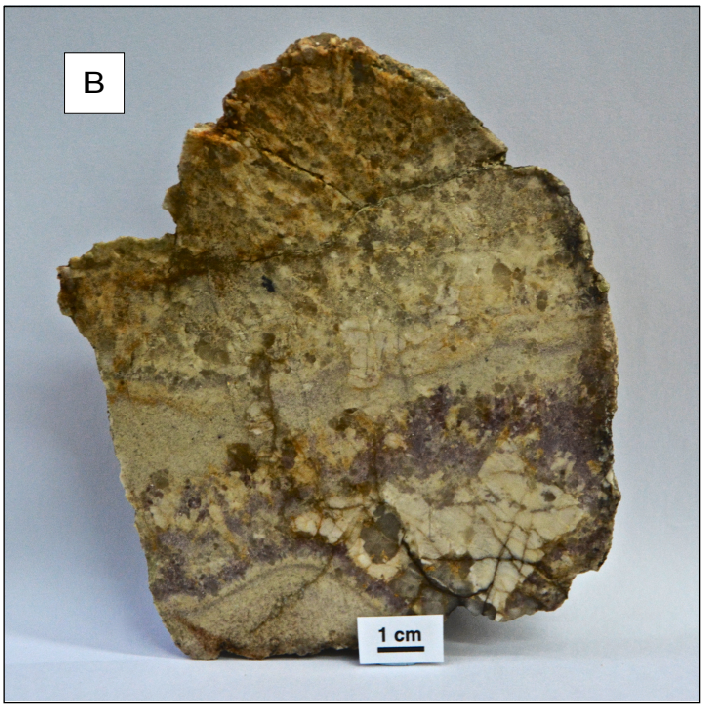
B
1 cm

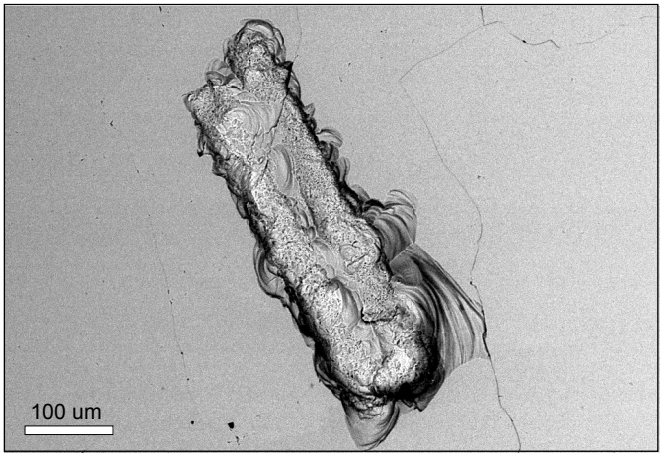
100 um

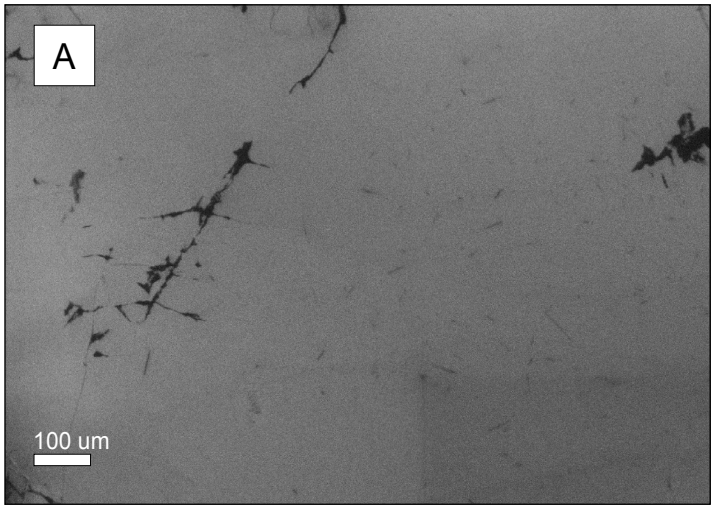
A
100 um

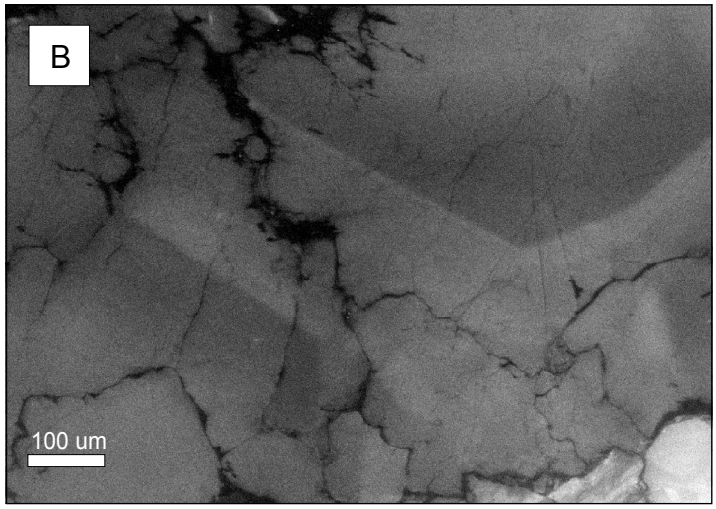
B
100 um

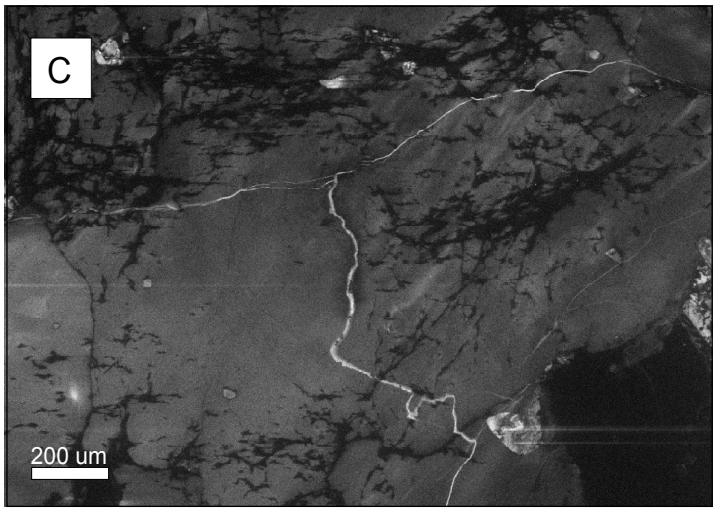
C
200 um

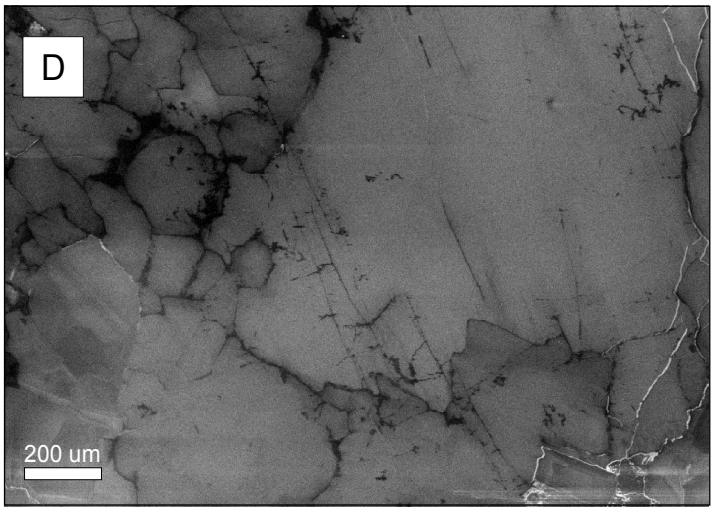
D
200 um

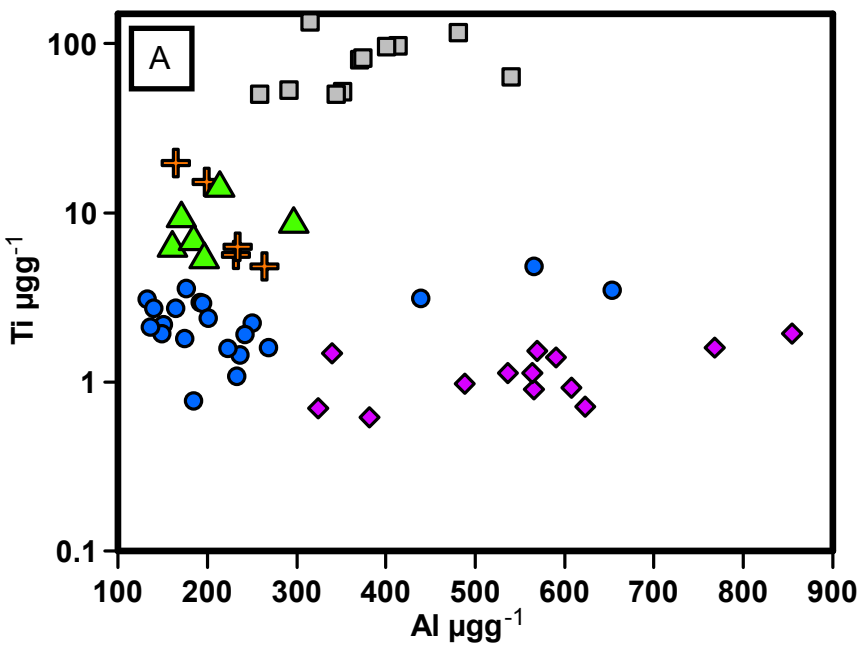

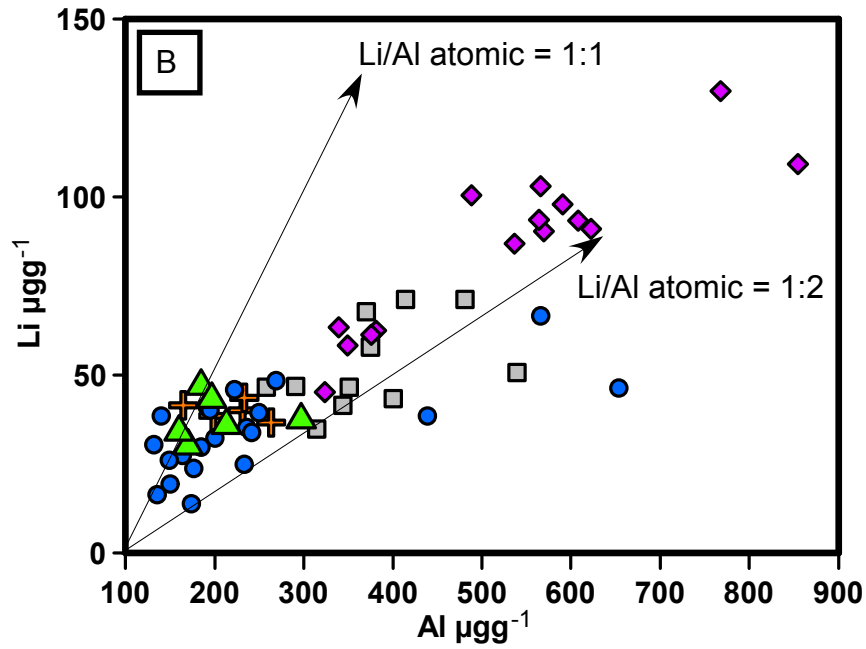

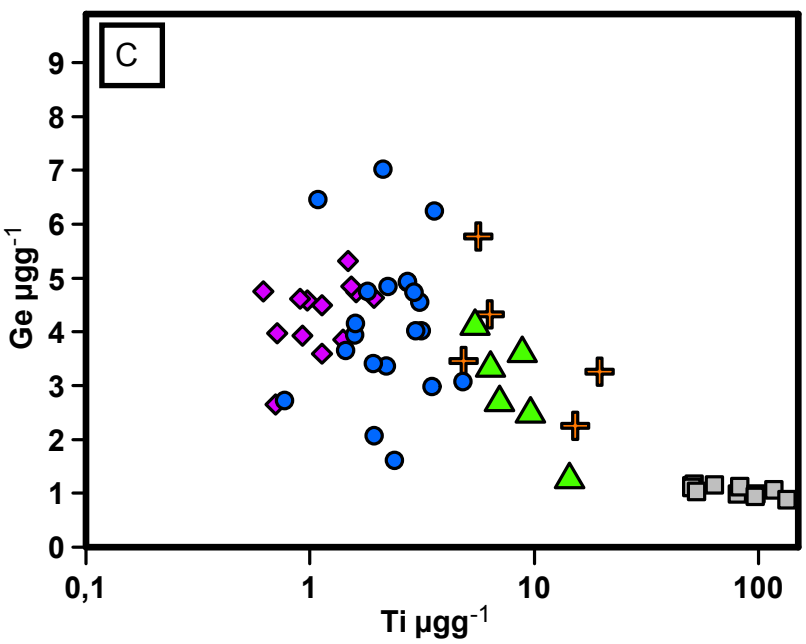

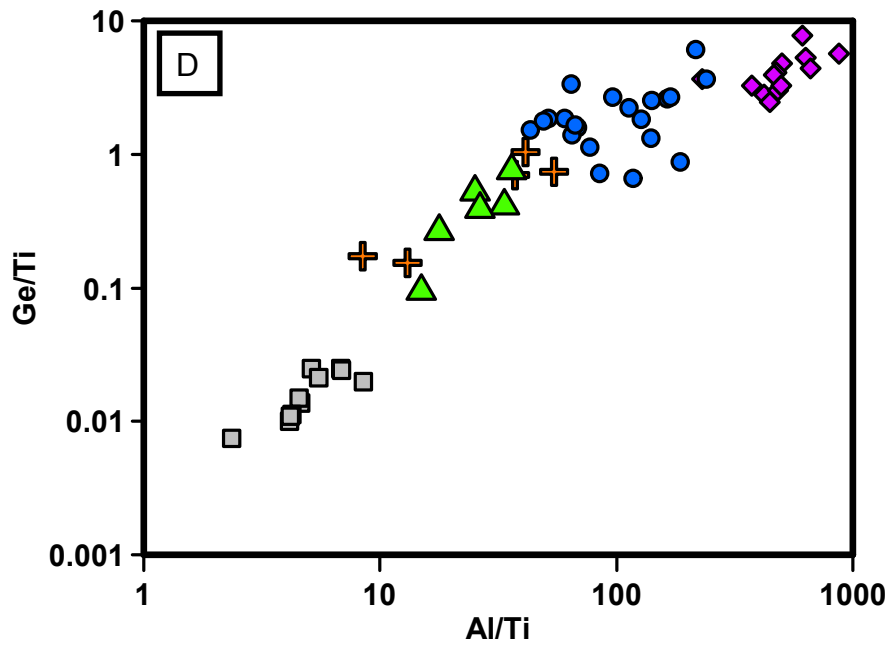

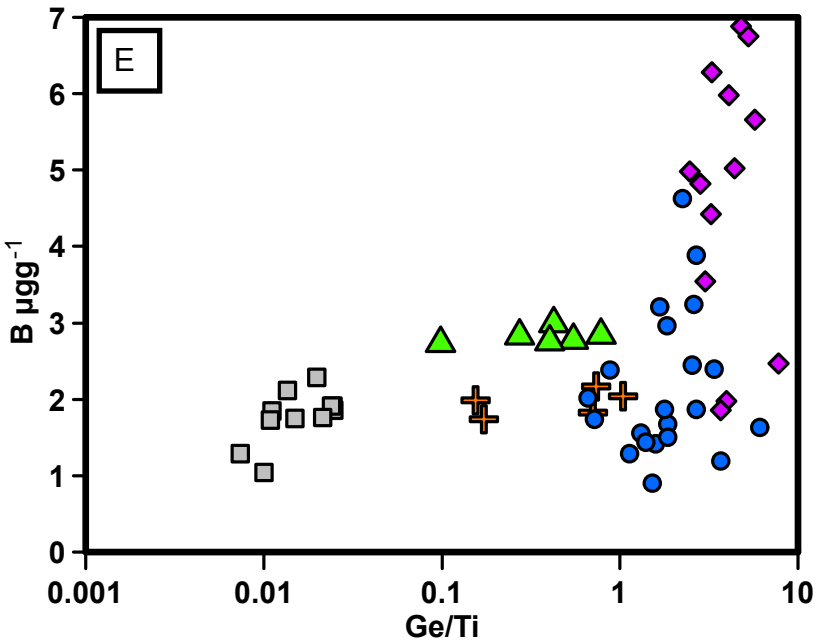

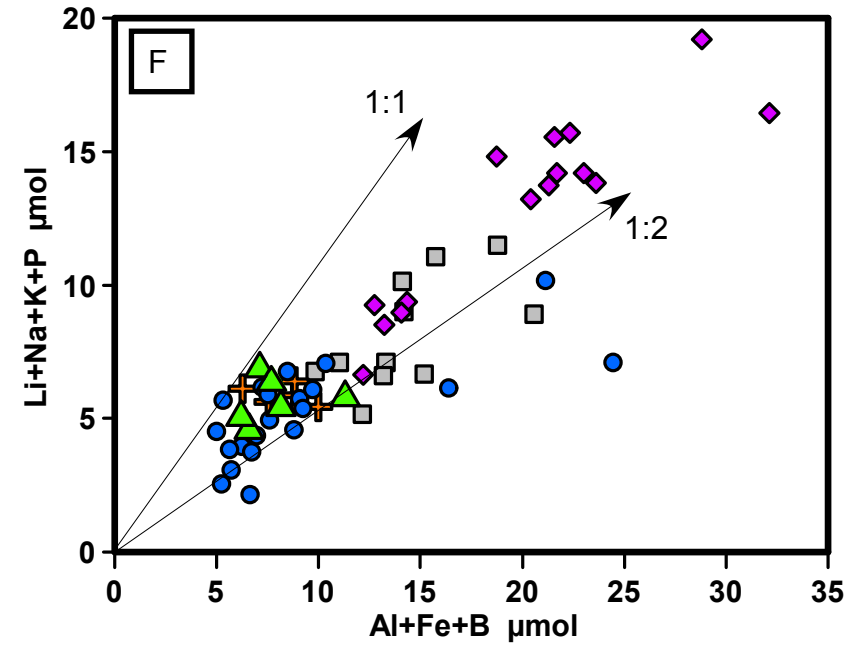

Monzogranite
Marginal granitic facies
Barren aplite-pegmatites
Intermediate aplite-pegmatites
Li-rich aplite-pegmatites

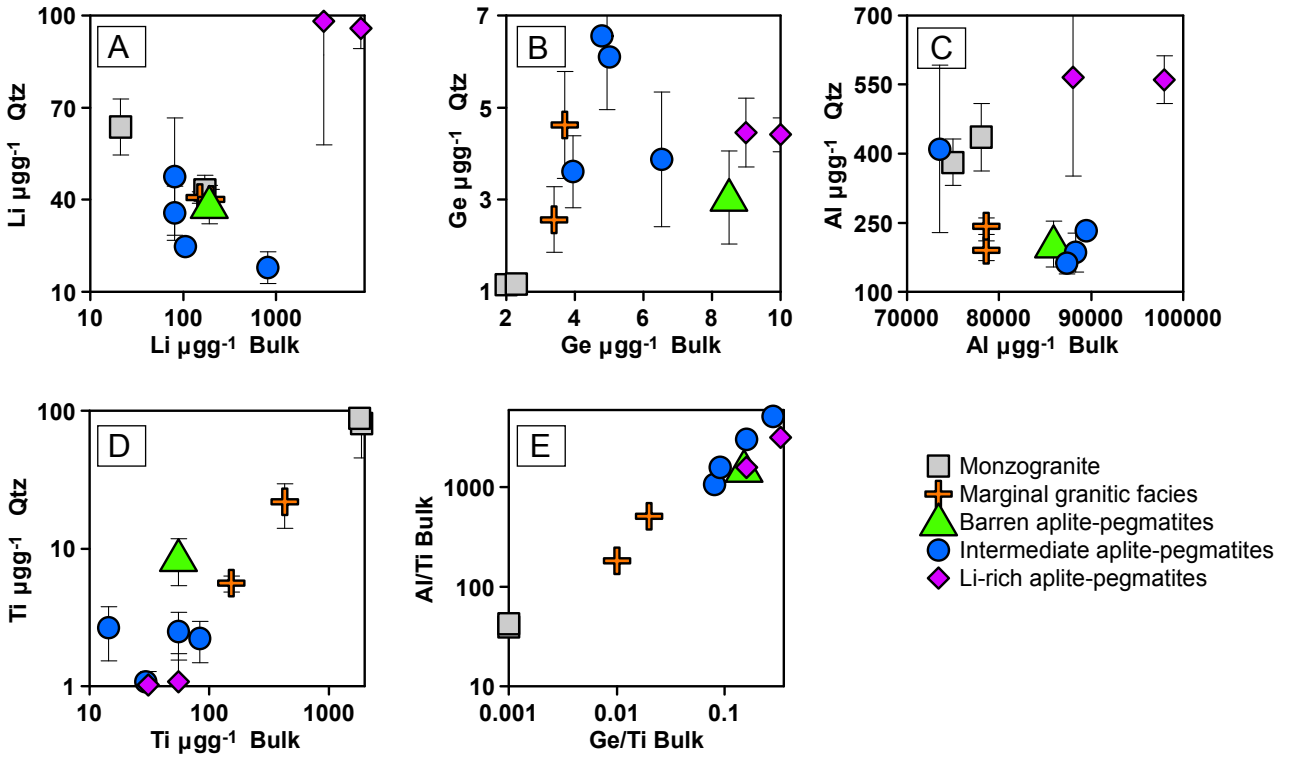
A
Li µgg-1 Qtz
Li µgg-1 Bulk
B
Ge µgg-1 Qtz
Ge µgg-1 Bulk
C
Al µgg-1 Qtz
Al µgg-1 Bulk
D
Ti µgg-1 Qtz
Ti µgg-1 Bulk
E
Al/Ti Bulk
Ge/Ti Bulk
Monzogranite
Marginal granitic facies
Barren aplite-pegmatites
Intermediate aplite-pegmatites
Li-rich aplite-pegmatites

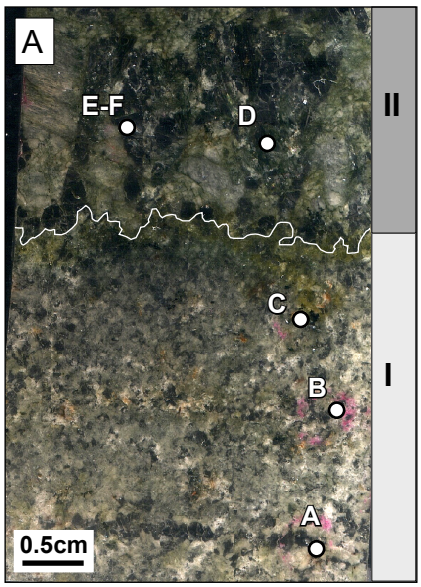

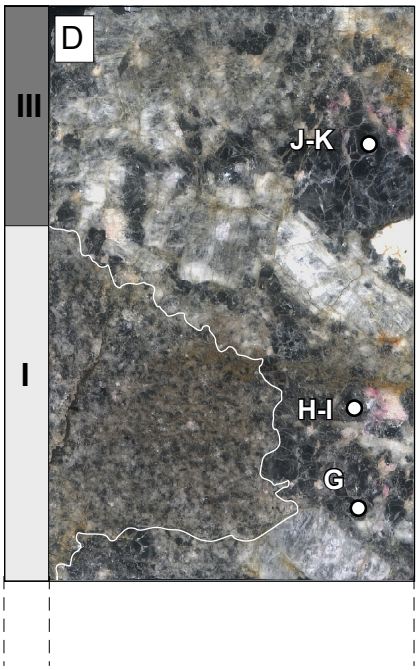

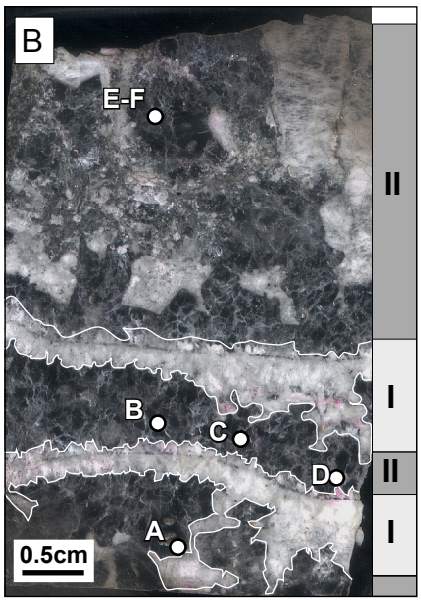

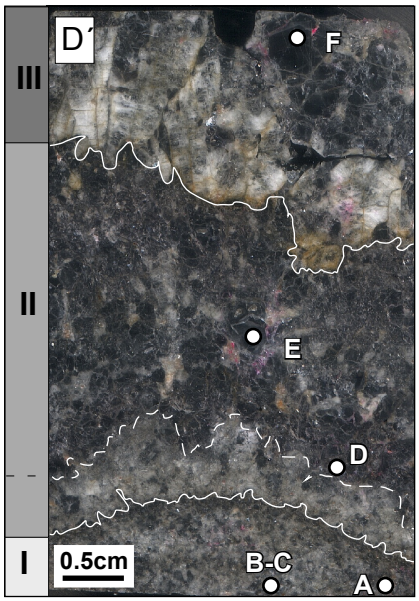

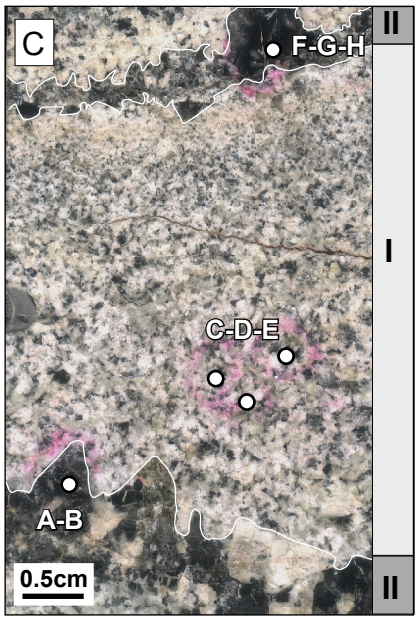

Type I (very fine-grained layers)

Type II (fine-grained layers)

Type III (medium-grained layers)

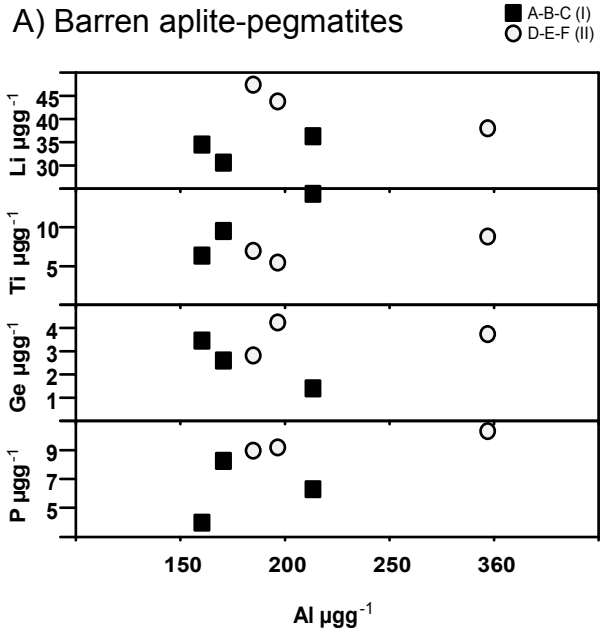
A) Barren aplite-pegmatites
A-B-C (I)
D-E-F (II)
Li µgg-1
Ti µgg-1
Ge µgg-1
P µgg-1
Al µgg-1

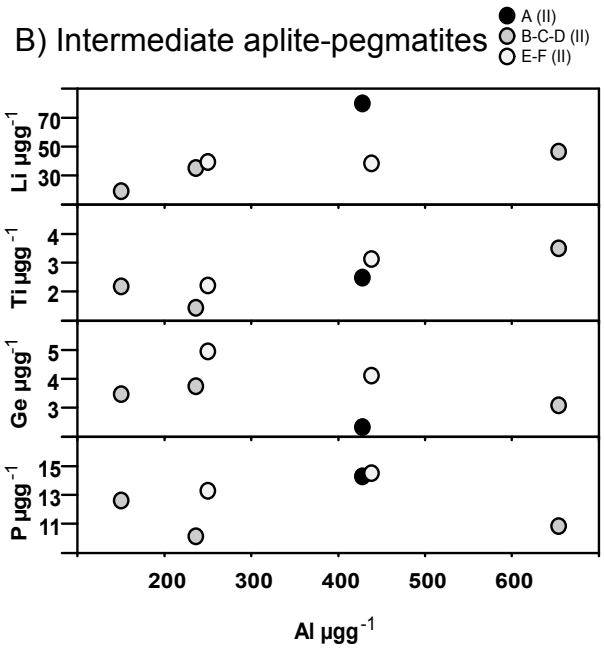
B) Intermediate aplite-pegmatites
A (II)
B-C-D (II)
E-F (II)
Li µgg-1
Ti µgg-1
Ge µgg-1
P µgg-1
Al µgg-1

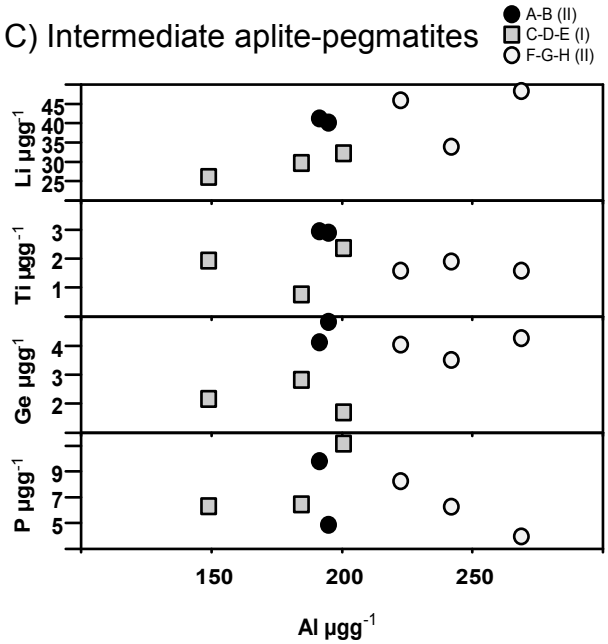
C) Intermediate aplite-pegmatites
A-B (II)
C-D-E (I)
F-G-H (II)
Li µgg-1
Ti µgg-1
Ge µgg-1
P µgg-1
Al µgg-1

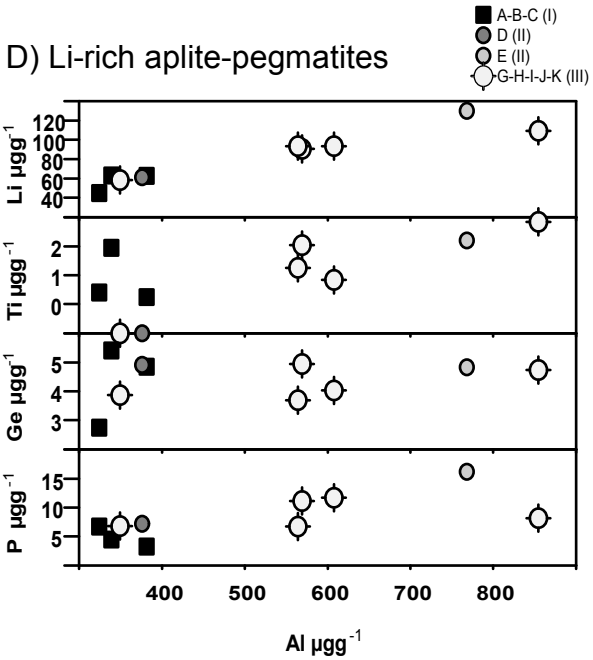
D) Li-rich aplite-pegmatites
A-B-C (I)
D (II)
E (II)
G-H-I-J-K (III)
Li µgg-1
Ti µgg-1
Ge µgg-1
P µgg-1
Al µgg-1

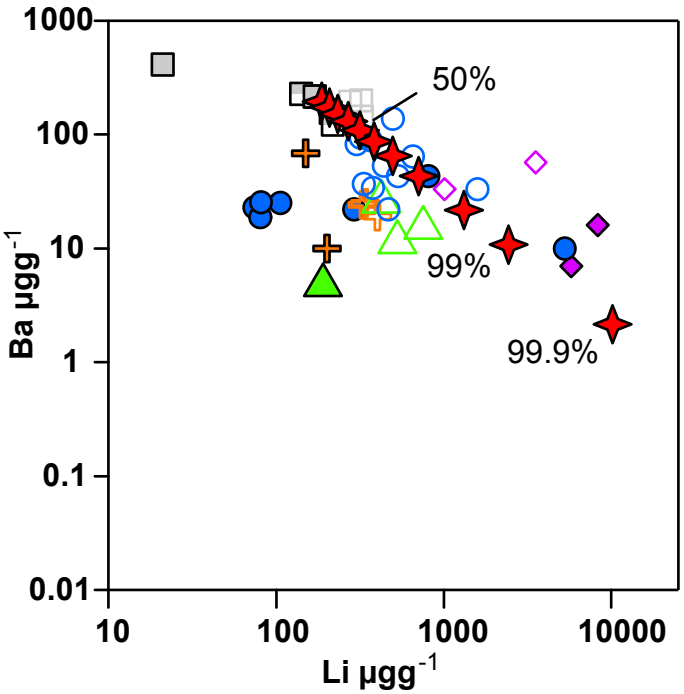

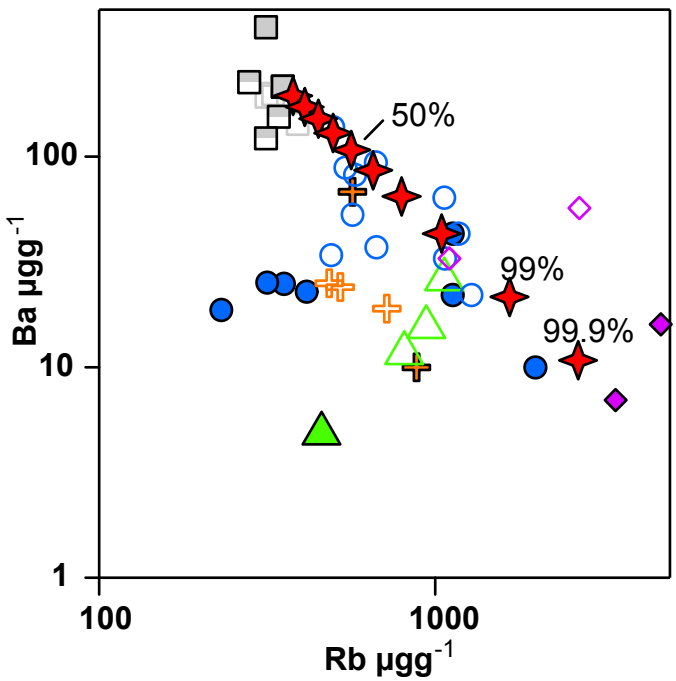

Monzogranite
Marginal granitic facies
Barren aplite-pegmatites
Intermediate aplite-pegmatites
Li-rich aplite pegmatites
Path of fractional crystallization

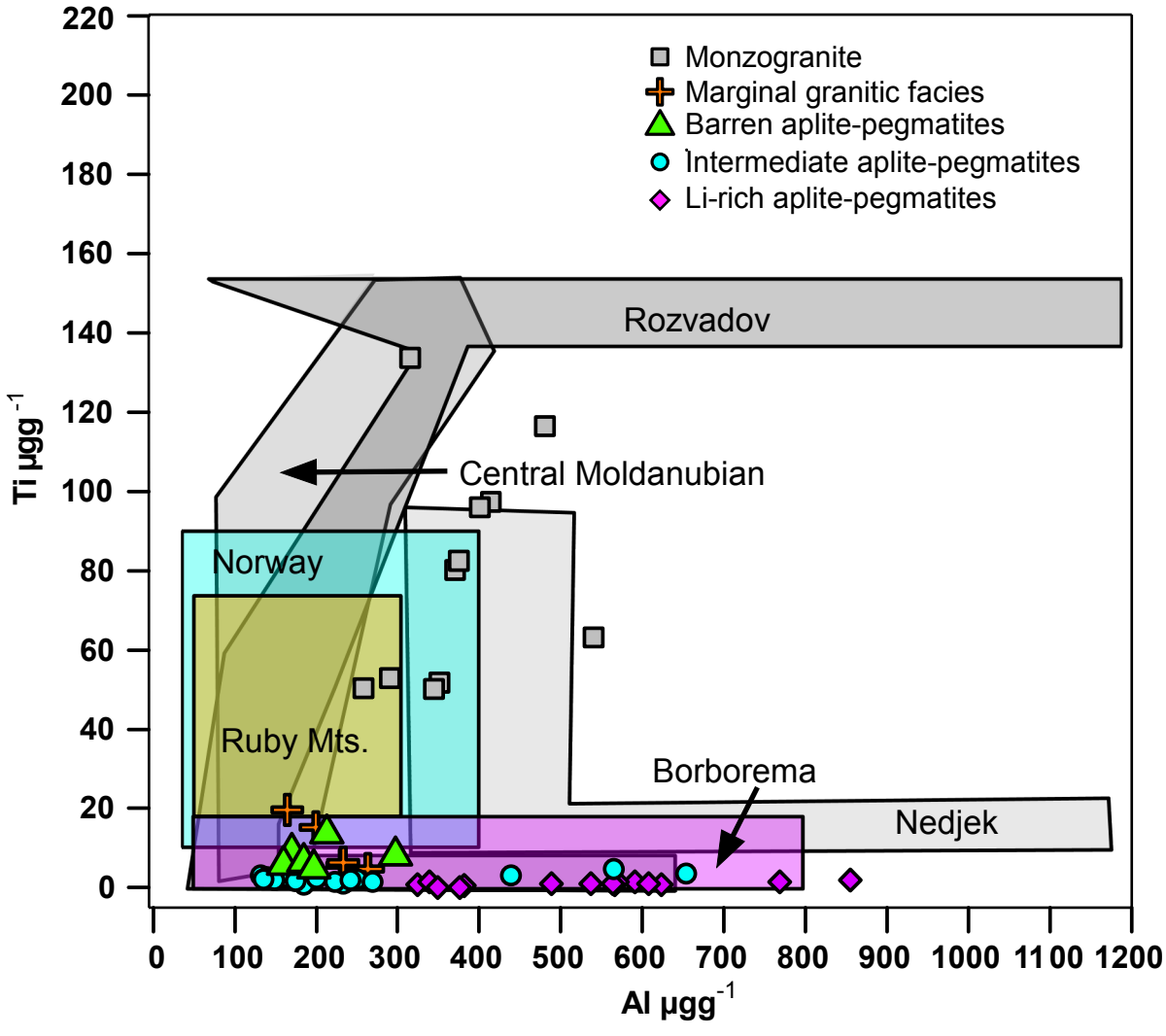
Monzogranite
Marginal granitic facies
Barren aplite-pegmatites
Intermediate aplite-pegmatites
Li-rich aplite-pegmatites
Rozvadov
Central Moldanubian
Norway
Ruby Mts.
Borborema
Nedjek
Ti µgg-1
Al µgg-1
0
20
40
60
80
100
120
140
160
180
200
220
0
100
200
300
400
500
600
700
800
900
1000
1100
1200

LITHOLOGY	MINERALOGY	QUARTZ GRAIN SIZE	QUARTZ HABIT	ROCK TEXTURE (quartz texture)
Porphyritic monzogranite	Quartz, K-feldspar, plagioclase, biotite, muscovite, cordierite, andalusite, tourmaline, zircon, apatite, oxides	Fine to medium 0.1-1 cm	Subrounded Anhedral Subhedral	Oriented porphyritic feldspar crystals Oxides and zircon (with metamictic halos) crystals usually inside or close to biotitte. (Quartz with undulose extinction)
Marginal granitic facies	Quartz, K-feldspar, plagioclase, tourmaline, biotite, cordierite, andalusite, muscovite, Fe-Li-muscovite, ilmenite,	Very fine to fine 0.1-0.5 cm	Subrounded Anhedral	Biotite frequently concentrated in layers, Biotite-Muscovites intergrowths. Accessory tourmaline prisms Aplitic texture Chloritization and serizitation of the Al-silicates (Single quartz crystals with undulatory extinction +anhedral quartz aggregates+ very fine (<2 mm) inclusions in tourmaline)
Barren aplite-pegmatites	Quartz, plagioclase, K-feldspar, muscovite, tourmaline, zinnwaldite, topaz, Fe-Mn phosphates, apatite, Sn-Nb-Ta oxides	Very fine to medium Pegmatitic layers: <3 cm Aplitic layers: <0.5 cm	Subrounded Anhedral	Layered texture, alternating pegmatitic and aplitic layers Locally greenish color in hand sample due to Fe-Mn phosphates (Single quartz crystals + anhedral quartz aggregates+ quartz occasionally occurs as comb shaped aggregates of very fine sized subrounded crystals (<0.3cm) + very fine inclusions in tourmaline and feldspar)
Intermediate aplite-pegmatites	Quartz, plagioclase, K-feldspar, muscovite, topaz, Li-Al phosphates, Fe-Mn phosphates, Sn-Nb-Ta oxides, apatite	Very fine to medium 0.1 – 2.5 cm	Subrounded Anhedral Largest ones: elongated	Simple pattern layering, alternating albite rich layers with quartz rich layers, the grain size also may change. Albite radial small flakes (Single quartz crystal with irregular contact some of them showing a weak undulose extinction +quartz occasionally occurs as comb shaped aggregates (up to 2.5 cm) of fine sized subrounded crystals (<0.5 cm))
Li-rich aplite-pegmatite	Quartz, plagioclase, K-feldspar, Li-Al-mica, topaz, Li-Al phosphates, Sn-Nb-Ta oxides, apatite	Very fine to medium 0.1- 1 cm	Anhedral Subrounded	Rhythmic layering, some with a complex pattern, with alternating albite-rich and Li-mica rich layers. Fan-shaped micas with patchy-zoning (Single quartz crystals in aplitic layers+ subrounded quartz aggregates, <0.8 cm)

Very fine< 3mm; Fine=3-6mm; Medium>6mm

Elements	Li	Be	B	Mn	Ge	Rb	Sr	Sb	U	Na	Al	P	K	Ca	Ti	Fe	Zn	Ga
LOD	0.07	0.03	1.7	0.02	0.21	0.03	0.02	0.02	0.02	10.5	4.9	2	18.5	5.6	0.84	0.62	1.1	0.03

Lithology		N	Li	Be	B	Ge	Al	P	K	Ti	Fe
Monzogranite	Average	11	52.5	0.1	1.8	1.2	376	2.7	20.1	79.5	14.7
	Std dev		12.6	0.1	0.3	0.1	81	1.4	17.1	28.9	12.4
Marginal granitic facies	Average	5	40	0.1	2	3.9	218	3.1	0.7	10.3	0.2
	Std dev		2.6	0.1	0.2	1.3	38	0.5	0.7	6.7	0.1
Barren aplite-pegmatites	Average	6	38.4	0.1	2.8	3	204	5.6	1.7	8.6	0.1
	Std dev		6.2	0.1	0.1	1	49	2.2	1.7	3.2	0.1
Intermediate aplite-pegmatites	Average	21	34.2	0.1	2.2	4.3	243	6.6	3.3	2.4	0.2
	Std dev		12.2	0.1	1	1.4	140	6.6	4.2	0.9	0.2
Li-rich aplite-pegmatites	Average	15	85.7	0.2	4.3	4.4	529	4.2	13.6	1	0.1
	Std dev		23	0.1	1.8	0.7	157	3.1	15.7	0.5	0.1

Lithology	Layer type	Spot		Li	Be	B	Ge	Al	P	K	Ti	Fe	Al/Ti	Ge/Ti
Barren	Type II	A-B-C	Avg	33.8	-	2.8	2.5	181.4	6	0.8	10.1	0.1	19.3	0.3
aplite-pegmatites			*Std dev*	2.9	-	0.1	1	28.1	1.3	1	4	0.1	5.3	0.2
	Type II	D-E-F	Average	43.1	-	2.9	3.6	226.1	5.2	2.6	7.1	0.1	32.1	0.5
			Std dev	4.8	-	0.1	0.7	61.6	3.1	2	1.7	0.1	5	0.2
Intermediate	Type II	A	Avg	66.7	0.3	2	3.2	565.4	13.8	4.1	4.8	0.3	117.4	0.7
aplite-pegmatites	Type II	B-C-D	Avg	33.7	0.2	2.4	3.4	346.7	8.7	3.2	2.4	0.1	139.8	1.7
			Std dev	13.6	0.1	0.9	0.3	269.3	1.8	1.5	1	0.1	62.6	0.9
	Type II	E-F	Avg	38.8	0.2	3.1	4.5	344.2	8.4	9.1	2.7	0.1	126.4	1.8
			Std dev	0.7	0	2.2	0.6	133.3	8.4	5	0.6	0	19.3	0.6
	Type II	A-B	Avg	40.7	0	2.3	4.5	193.1	3.4	2.6	2.9	0.2	66.1	1.5
			Std dev	0.8	0.1	1.3	0.5	2.3	3.5	0.8	0	0.1	1.5	0.2
	Type I	C-D-E	Avg	29.4	-	1.4	2.2	178	4	0.8	1.7	0.2	0.4	134.2
			Std dev	3.1	-	0.3	0.6	26.4	2.8	1.3	0.8	0.1	0.4	92.1
	Type II	F-G-H	Avg	42.7	0.2	3.1	3.9	244.4	2.2	7	1.7	0.4	0	145.6
			Std dev	7.7	0	0.7	0.4	23.2	2.1	8.8	0.2	0.2	0	21.7
Li-rich	Type I	A-B-C	Avg	56.9	0.1	2.1	4.3	348.2	0.8	3.3	0.9	0	436	5.1
aplite-pegmatites			*Std dev*	10.3	0.1	0.3	1.4	29.7	1.7	1.5	0.5	0.1	192.1	2.3
	Type II	D	Avg	61.2	0.1	1.4	4.9	376	3.2	2.2	0	0	0	0
	Type II	E	Avg	129.8	0.3	3.5	4.8	768	12.2	4.8	1.6	0.2	481.2	3
	Type III	F-G-H-I-J	Avg	89	0	4.7	4.3	589.1	4.9	11.2	1.1	0.2	495.6	3.3
			Std dev	18.7	0.2	1.2	0.6	179.8	2.4	13.3	0.7	0.1	123.1	0.8

	Mineral modes (vol. %)	Partition coefficients		
	Albuquerque	Li	Rb	Ba
Quartz	36	0.05	0.01	0.025
K-Feldspar	29	0.05	0.7	6
Plagioclase	29	0.05	0.1	0.3
Biotite	3	1,65	2	3
Muscovite	2	0.8	1.4	3.7